1989

Computation of transonic flows using a streamfunction coordinate system.

Rana Khalid. Naeem
University of Windsor

NOTICE

The quality of this microform is heavily dependent upon the quality of the original thesis submitted for microfilming. Every effort has been made to ensure the highest quality of reproduction possible.

If pages are missing, contact the university which granted the degree.

Some pages may have indistinct print especially if the original pages were typed with a poor typewriter ribbon or if the university sent us an inferior photocopy.

Reproduction in full or in part of this microform is governed by the Canadian Copyright Act, R.S.C. 1970, c. C-30, and subsequent amendments.

AVIS

La qualité de cette microforme dépend grandement de la qualité de la thèse soumise au microfilmage. Nous avons tout fait pour assurer une qualité supérieure de reproduction.

S'il manque des pages, veuillez communiquer avec l'université qui a conféré le grade.

La qualité d'impression de certaines pages peut laisser à désirer, surtout si les pages originales ont été dactylographiées à l'aide d'un ruban usé ou si l'université nous a fait parvenir une photocopie de qualité inférieure.

La reproduction, même partielle, de cette microforme est soumise à la Loi canadienne sur le droit d'auteur, SRC 1970, c. C-30, et ses amendements subséquents.

COMPUTATION OF TRANSONIC FLOWS USING A STREAMFUNCTION COORDINATE SYSTEM

by

© Rana Khalid Naeem

A Dissertation
Submitted to the Faculty of Graduate Studies and Research
through the Department of Mathematics and Statistics
in Partial Fulfillment of the Requirements for the
Degree of Doctor of Philosophy at
The University of Windsor

Windsor, Ontario, Canada

1988

ISBN 0-315-50519-2

Dedicated to my parents, Rana Habib-ur-Rahman and Hakeemun (Zarina Parveen)

ABSTRACT

COMPUTATION OF TRANSONIC FLOWS USING A STREAMFUNCTION COORDINATE SYSTEM

by

Rana Khalid Naeem

This dissertation studies steady two-dimensional transonic flows past symmetric airfoils.

The flow equations are first transformed into (ϕ,ψ) curvilinear coordinates, where $\psi(x,y)$ is the streamfunction and $\phi(x,y)$ is arbitrary, and then to von Mises variables (x,ψ). Flows over symmetric profile at zero and non-zero angles of attack are formulated in terms of the independent variables (x,ψ), providing a rectangular computational domain with Dirichlet boundary conditions. The flow equations in unknowns $y(x,\psi)$ and $\rho(x,\psi)$ are discretized using a finite difference method, producing a system of algebraic equations which is solved by SLOR. The surface pressure coefficient is computed on airfoils at subcritical and supercritical Mach numbers. The present results are in good agreement with available results in the literature. In the (x,ψ) system, the airfoil design problem is conveniently formulated as a Newmann boundary value problem and solved numerically to produce the required body shape.

The need to solve a sequence of direct problems is eliminated.

This dissertation provides simple and fast algorithms for the computation of the flows described above.

ACKNOWLEDGMENTS

The author expresses his sincere gratitude, appreciation and admiration to Dr. R. M. Barron for his inspiration, encouragement and advice throughout this work.

The author is grateful to Dr. R. M. Barron, Chairman, Department of Mathematics and Statistics, for providing him with a Graduate teaching assistanship and a research assistantship.

Finally, I wish to thank my parents, brothers and sister for their encouragement, advice and moral support throughout my studies.

TABLE OF CONTENTS

LIST OF FIGURES

LIST OF TABLES

LIST OF DIAGRAMS

NOMENCLATURE

a, a_∞	local and free stream speed of sound
C_L	lift coefficient
C_p	pressure coefficient
CPU	upper surface pressure coefficient
CPL	lower surface pressure coefficient
E, F, G	coefficients of first fundamental form
J	Jacobian of transformation
L	characteristic length
M, M_∞	local Mach and free stream Mach numbers
$\bar{p}, p$	dimensional and nondimensional pressure
$\bar{u}, u$ U_∞	dimensional and nondimensional x-component of velocity and free stream speed of fluid
$\bar{v}, v$	dimensional and nondimensional y-component of velocity
$\bar{V}, V$	dimensional and nondimensional speed
$\bar{x}, \bar{y}$, x, y	dimensional and nondimensional Cartesian coordinates
x_{LE}	value of x at the leading edge
x_{TE}	value of x at the trailing edge
α	angle of attack
β	local angle of inclination of streamline with x-axis
γ	adiabatic constant
Γ	circulation
Γ^k_{ij}	Christoffel symbols; i,j,k are integers

ψ	curvilinear coordinate , streamfunction
ϕ	curvilinear coordinate
Φ	velocity potential
ξ	stretched coordinate in x-direction
ξ_{LE}	value of ξ at the leading edge
ξ_{TE}	value of ξ at the trailing edge
η	stretched coordinates in ψ-direction
$\bar{\rho}, \rho$	dimensional and nondimensional density
ρ_I	density in artificial compressibility method
$\tilde{\rho}$	modified density
μ	switching function
$\bar{\omega}, \omega$	dimensional and nondimensional vorticity

CHAPTER I

INTRODUCTION

The three basic tools used by researchers to gain an understanding of the various physical phenomena associated with fluid flow are mathematical analysis, experimentation or testing and numerical computation. Before the development of computers, researchers relied heavily on fairly simple mathematical models and analysis to provide guidelines for experimentalists, who developed various devices to make measurements of flow quantities of particular interest to them. As the design of modern engineering hardware has become more and more sophisticated there has been a greater demand for more detailed and accurate flow field information. This need, together with the advancements made in high-speed computing, have made computational methods an equal partner with experimental methods in efforts to analyze complicated flow situations.

Information about recent advances in experimental techniques can be obtained in references [1-8]. The present dissertation is concerned with the numerical computation of transonic flows. As background information we summarize some of the important analytical and

computational work dealing with transonic flows.

Analytic methods have been developed for the determination of transonic flow fields past bodies, but these methods have serious limitations. A thorough survey is provided by Cheng [7], but we only discuss briefly the two best known methods. One of the well-known analytical methods is the hodograph method in which the flow equations are studied in the plane of the velocity components. A wide variety of solutions can be constructed, but this method has some serious drawbacks. In particular, the shape of the airfoil cannot be prescribed in advance and shock waves cannot be treated. Furthermore, the shape of the airfoil changes significantly if either the free stream Mach number or thickness ratio is slightly altered. The solutions obtained using this method, however, provide important checkpoints for the validation of numerical algorithms or experimental results. The perturbation method is also a well known method used to study fluid flows. In this method the dependent variables are usually expressed in a power series of some parameter. The parameter may be a function of thickness ratio or Mach number or both. References to work done using this method can be obtained from Van Dyke[9]. Hafez [10] has recently developed an analytic perturbation analysis

for transonic flows with shock waves and has discussed how the formation and disappearance of shocks can be easily handled.

Much of the early work in compressible flow uses a formulation in terms of the velocity potential and most books treat linearized subsonic and supersonic flows in this way, see for example, [6]. The full-potential equation is obtained by assuming inviscid, irrotational and isentropic conditions. These assumptions greatly simplify the equations, reducing the momentum equations to a single relation (Bernoulli's equation) between fluid density and velocity. The introduction of the velocity potential into the continuity equation provides a single second-order quasi-linear equation of mixed elliptic-hyperbolic type, depending upon the value of the local Mach number.

In 1970, the search for more realistic solutions for transonic flow fields led to the application of numerical methods to the equations for steady compressible potential flow. Murman and Cole [11] are the first to have achieved a stable transonic solution for the two-dimensional transonic small-disturbance equation using central differencing in the subsonic region and upwind differencing in the supersonic region. Ballhaus and Bailey [12] have carried out the extension to three-dimensional transonic small-disturbance flows.

For the full-potential equation in two dimensions, numerical procedures have been given by Steger and Lomax [13], Garabedian and Korn [14] and others. The extension to three dimensions has been presented by Jameson and Caughey [15,16]. Field methods can also be used to study transonic flows and a full survey of these methods is given in [16,18].

Besides the potential formulation, the stream function formulation can also be used to study transonic flows. The streamfunction formulation is capable of producing accurate and inexpensive solutions to rotational transonic flow problems [19]. In the past, streamfunction methods have been based on Crocco's equation. Such an equation models the rotational effects correctly and yields the correct shock jump condition provided the correct density jump is specified. However, the method requires knowledge of the vorticity. When a shock is present, the vorticity is introduced at the shock in a discontinuous manner and this can result in numerical inaccuracies. To overcome these difficulties one requires a formulation which does not require knowledge or explicit evaluation of the vorticity. Such a formulation is obtained by considering density and streamfunction as dependent variables. For adiabatic flows, in the above mentioned formulation, the

governing equations are the momentum equations, which do not explicitly depend on the vorticity. The other advantage of the streamfunction formulation is that some boundary conditions are simpler to implement. In particular, the tangency condition at the airfoil surface is expressed by specifying the streamfunction ψ equal to some constant on the body.

The streamfunction formulation is also convenient for implementation of the Kutta condition for lifting flows. For C-grids, common in numerical grid generation, the Kutta condition is implemented by setting ψ on the body equal to ψ at the first-point off the trailing edge. The main difficulty with the streamfunction formulation is that the density is not uniquely determined in terms of the mass flux. To overcome this difficulty, artificial viscosity and artificial density methods have been developed and these methods with appropriate references are briefly discussed in Chapter III.

Techniques such as the methods of conjugate gradients (CG) [20] and approximate factorization (ADI, AF2, SIP) [20] are also employed to study transonic flows. A very popular method employed nowadays in the numerical solution of partial differential equations is the numerical grid generation. In this method a curvilinear grid is generated in the flow domain, independent of the flow

field, and then the governing equations are solved on this body-conforming grid. Extensive work in transonic flow has been done employing grid generation. The method is described in detail in an excellent article by Thompson, Warsi, Mastin [21].

Also in the early 1970's Martin [22] introduced a curvilinear coordinate system (ϕ,ψ), where ψ is the streamfunction, to study the geometry of certain incompressible viscous two-dimensional flows. This formulation has been used by Grossman and Barron [23] to numerically investigate incompressible irrotational inviscid flow over symmetric airfoils at zero angle of incidence. They have chosen the coordinate system to be orthogonal, which implies that the curves $\phi(x,y)$ = constant are potential curves. In this case it is not possible to analytically determine the images of the leading and trailing edges in the (ϕ,ψ) system. Numerically obtained values for the locations of the leading and trailing edges are not very accurate, resulting in inaccuracies in the solution near these edges. During a further study of inviscid incompressible irrotational flows, Barron [24] has introduced von Mises variables (x,ψ). Using these independent variables one knows exactly where the leading and trailing edges are mapped in the (x,ψ)-plane and inaccuracies in the solution near these points can be

eliminated. Furthermore, as in the work of Grossman and Barron [23], this formulation automatically provides a rectangular computational domain (x,ψ) and the need to do numerical grid generation is avoided.

This dissertation proposes a new method, based on that of Barron [24], for studying subcritical and supercritical flows at zero and non-zero angles of attack. The method utilizes von Mises variables (x,ψ) which conveniently provides a Dirichlet formulation for the direct problem and circumvents the need to do grid generation. In the present study only irrotational, isentropic inviscid flows are considered. Now we briefly describe each of the chapters of the dissertation.

In Chapter II we derive the inviscid compressible flow equations in the (ϕ,ψ) and (x,ψ) systems. Chapter III gives the flow equations in non-stretched and stretched coordinates with appropriate boundary conditions for flow over an arbitrary airfoil at zero incidence. The introduction of artifical compressibility or modified density into the flow equations is discussed and the numerical algorithm is presented. Difficulties associated with the artificial compressibility method are discussed, particularly the problem of achieving convergence on finer grids, as is well-documented in the literature. This problem is resolved by expressing the flow equations in an alternate

form and applying type-dependent differencing. The chapter concludes with a discussion of the results for several subcritical and supercritical cases. Chapter IV presents the flow equations in un-stretched and stretched coordinates along with appropriate boundary conditions for the design or inverse problem and the computed results are compared with exact results. Chapter V deals with lifting airfoils in incompressible and compressible flows. The flow equations together with boundary conditions are presented and a numerical algorithm is given. The calculated results are compared with values obtained experimentally or by other numerical methods.

CHAPTER II

FLOW EQUATIONS

2.1 FLOW EQUATIONS

The steady two-dimensional flow of an inviscid compressible fluid, in the absence of body forces, is governed by the following equations:

$$(\bar{\rho}\bar{u})_{\bar{x}} + (\bar{\rho}\bar{v})_{\bar{y}} = 0 \qquad \text{(continuity)} \qquad (2.1.1)$$

$$\begin{aligned} &\bar{\rho}(\bar{u}\bar{u}_{\bar{x}} + \bar{v}\bar{u}_{\bar{y}}) + \bar{p}_{\bar{x}} = 0 \\ &\bar{\rho}(\bar{u}\bar{v}_{\bar{x}} + \bar{v}\bar{v}_{\bar{y}}) + \bar{p}_{\bar{y}} = 0 \end{aligned} \qquad \text{(momentum equations)} \qquad (2.1.2)$$

These equations constitute a system of non-linear partial differential equations in four unknown functions: $\bar{\rho}$ the density, $\bar{p}$ the pressure, $\bar{u}$ and $\bar{v}$ the velocity components, all functions of $\bar{x}$, $\bar{y}$. The bar (-) indicates that the quantity is dimensional. The state and energy equations along with (2.1.1, 2.1.2) constitute a complete system of equations.

Equation (2.1.2) can be rewritten as

$$\begin{aligned} &\left[\frac{\bar{V}^2}{2} + \frac{\bar{p}}{\bar{\rho}}\right]_{\bar{x}} - \bar{v}\bar{\omega} + \frac{\bar{p}\,\bar{\rho}_{\bar{x}}}{\bar{\rho}^2} = 0 \\ &\left[\frac{\bar{V}^2}{2} + \frac{\bar{p}}{\bar{\rho}}\right]_{\bar{y}} + \bar{u}\bar{\omega} + \frac{\bar{p}\,\bar{\rho}_{\bar{y}}}{\bar{\rho}^2} = 0 \end{aligned} \qquad (2.1.3)$$

wherein,

$$\bar{V}^2 = \bar{u}^2 + \bar{v}^2 \quad \text{(speed)}$$

$$\bar{\omega} = \bar{v}_{\bar{x}} - \bar{u}_{\bar{y}} . \quad \text{(vorticity)} \qquad (2.1.4)$$

For convenience in the analysis, the flow equations are non-dimensionalized by introducing non-dimensional variables x,y,u,v,ρ,ω,p through relations

$$\bar{x} = xL$$
$$\bar{y} = yL$$
$$\bar{u} = u_\infty u$$
$$\bar{v} = u_\infty v$$
$$\bar{\rho} = \rho_\infty \rho$$
$$\bar{\omega} = \omega u_\infty / L$$
$$\bar{p} = p\rho_\infty u_\infty^2$$

where L, u_∞, ρ_∞ are, respectively, the characteristic length, the free stream speed and the density.

Employing the above relations in (2.1.1),(2.1.3) and (2.1.4), we obtain

$$(\rho u)_x + (\rho v)_y = 0 \quad \text{(continuity)} \qquad (2.1.5)$$

$$\left[\frac{V^2}{2} + \frac{p}{\rho}\right]_x - v\omega + \frac{p\rho_x}{\rho^2} = 0 \quad \text{(x-linear momentum equation)} \qquad (2.1.6)$$

$$\left[\frac{V^2}{2} + \frac{p}{\rho}\right]_y + u\omega + \frac{p\rho_y}{\rho^2} = 0 \quad \text{(y-linear momentum equation)} \qquad (2.1.7)$$

$$\omega = v_x - u_y \qquad \text{(vorticity)} \qquad (2.1.8)$$

where

$$V^2 = u^2 + v^2 \ . \qquad (2.1.9)$$

The equation of continuity (2.1.5) implies the existence of the streamfunction $\psi(x,y)$ such that

$$\rho u = \psi_y \ , \quad \rho v = -\psi_x \ . \qquad (2.1.10)$$

Following Martin's [22] approach, we introduce curvilinear coordinates ϕ,ψ, in which the curves ψ = constant are the streamlines and the curves ϕ = constant are left arbitrary so that the physical coordinates x,y can be replaced by ϕ,ψ.

Let

$$x = x(\phi,\psi), \quad y = y(\phi,\psi) \qquad (2.1.11)$$

define a system of curvilinear coordinates in the (x,y)-plane. The first fundamental form of differential element is defined by

$$ds^2 = E(\phi,\psi)d\phi^2 + 2F(\phi,\psi)d\phi d\psi + G(\phi,\psi)d\psi^2 \qquad (2.1.12)$$

in which E, F, G are given by

$$\begin{aligned} E(\phi,\psi) &= x_\phi^2 + y_\phi^2 \\ F(\phi,\psi) &= x_\phi x_\psi + y_\phi y_\psi \\ G(\phi,\psi) &= x_\psi^2 + y_\psi^2 \ . \end{aligned} \qquad (2.1.13)$$

Equations (2.1.11) can be solved to determine ϕ,ψ as functions of x,y so that

$$x_\phi = J\psi_y,\ y_\phi = -J\psi_x,\ x_\psi = -J\phi_y, y_\psi = J\phi_x \qquad (2.1.14)$$

provided $J\neq 0$, where J, the Jacobian of the transformation (2.1.11), is defined by

$$J = x_\phi y_\psi - x_\psi y_\phi \ . \qquad (2.1.15)$$

It is easy to show that equation (2.1.15) can be written as

$$J = \pm W \ , \quad W = \sqrt{EG - F^2} \ . \qquad (2.1.16)$$

Let $\beta(\phi,\psi)$ be the angle between the tangent vector (x_ϕ, y_ϕ) to the coordinate line ϕ = constant and the x-axis (see Figure 1), then

$$x_\phi = E^{1/2}\cos\beta \ , \quad y_\phi = E^{1/2}\sin\beta \ . \qquad (2.1.17)$$

Solving (2.1.13) and (2.1.17) for x_ψ and y_ψ, we find,

$$x_\psi = \frac{F}{E^{1/2}}\cos\beta - \frac{J}{E^{1/2}}\sin\beta$$
$$y_\psi = \frac{F}{E^{1/2}}\sin\beta + \frac{J}{E^{1/2}}\cos\beta \ . \qquad (2.1.18)$$

The integrability conditions for x and y are

$$x_{\psi\phi} = x_{\phi\psi} \ , \quad y_{\phi\psi} = y_{\psi\phi}$$

which, after some reductions with the help of (2.1.16), yield

$$\beta_\phi = \frac{J}{E}\,\Gamma^2_{11}$$

$$\beta_\psi = \frac{J}{E}\,\Gamma^2_{12}$$

where

$$\Gamma^2_{11} = \frac{-FE_\phi + 2EF_\phi - EE_\psi}{2W^2}$$

$$\Gamma^2_{12} = \frac{EG_\phi - FE_\psi}{2W^2}.$$

On computing the integrability condition for $\beta(\phi,\psi)$,

$$\beta_{\phi\psi} = \beta_{\psi\phi}$$

we find, after some simple manipulation,

$$K = \frac{1}{W}\left[\left(\frac{W}{E}\Gamma^2_{11}\right)_\psi - \left(\frac{W}{E}\Gamma^2_{12}\right)_\phi\right] = 0 \qquad (2.1.19)$$

where K is called the Gaussian curvature and equation (2.1.19) is called the Gauss equation. This equation represents a necessary and sufficient condition that E,F,G are coefficients of the first fundamental form (2.1.12).

Having recorded the above results which can be found in [22], we now consider equations (2.1.10) and (2.1.6) to (2.1.9) and transform them into the (ϕ,ψ) system.

Equation (2.1.10), upon employing (2.1.14), provides

$$x_\phi = J\rho u\,, \quad y_\phi = J\rho v \qquad (2.1.20)$$

which gives

$$\sqrt{E} = \pm J\rho V \qquad (2.1.21)$$

which is the equivalent form of the equation of continuity (2.1.5) and (+) or (-) sign indicates that the fluid flows towards higher or lower parametric values of ϕ, respectively, along the streamline [47,48].

Equations (2.1.6), (2.1.7), upon employing the chain rule for differentiation and equation (2.1.20), give

$$\left[\frac{V^2}{2} + \frac{p}{\rho}\right]_\psi \psi_x + \left[\frac{V^2}{2} + \frac{p}{\rho}\right]_\phi \phi_x - \frac{\omega y_\phi}{\rho J} + \frac{p}{\rho^2}[\rho_\psi \psi_x + \rho_\phi \phi_x] = 0 \qquad (2.1.22a)$$

and

$$\left[\frac{V^2}{2} + \frac{p}{\rho}\right]_\psi \psi_y + \left[\frac{V^2}{2} + \frac{p}{\rho}\right]_\phi \phi_y + \frac{\omega x_\phi}{\rho J} + \frac{p}{\rho^2}[\rho_\psi \psi_y + \rho_\phi \phi_y] = 0 \; . \qquad (2.1.22b)$$

Multiplying equations (2.1.22a) and (2.1.22b) by ψ_y, ψ_x, respectively, and subtracting, we get,

$$\left[\frac{V^2}{2} + \frac{p}{\rho}\right]_\phi + \frac{p\rho_\phi}{\rho^2} = 0 \; . \qquad (2.1.23a)$$

Again, multiplying equations (2.1.22a) and (2.1.22b) by ϕ_y, ϕ_x, respectively, and subtracting, we get,

$$\left[\frac{V^2}{2} + \frac{p}{\rho}\right]_\psi + \frac{\omega}{\rho} + \frac{p}{\rho^2} \rho_\psi = 0 \; . \qquad (2.1.23b)$$

The equations (2.1.23a), (2.1.23b) are the new equivalent forms of the linear momentum equations (2.1.6), (2.1.7), respectively.

Following Martin's development and using equation (2.1.21), the vorticity equation (2.1.8) in the (ϕ,ψ) system can be expressed as [47,48]

$$\omega = \frac{1}{W}\left[\left(\frac{F}{\rho W}\right)_{\phi} - \left(\frac{E}{\rho W}\right)_{\psi}\right] \quad . \tag{2.1.24}$$

Summing up the results of this section, we have

Theorem:

If the streamlines $\psi(x,y)$ = constant of the steady flow of an inviscid compressible fluid are considered as one set of coordinate lines in a curvilinear coordinate system (ϕ,ψ) in the physical plane, then the equations (2.1.5)-(2.1.8) transform to the following system of equations with ϕ,ψ as independent variables

$$\sqrt{E} = \rho V W \tag{2.1.25a}$$

$$\left[\frac{V^2}{2} + \frac{p}{\rho}\right]_{\phi} + \frac{p\rho_{\phi}}{\rho^2} = 0 \tag{2.1.25b}$$

$$\left[\frac{V^2}{2} + \frac{p}{\rho}\right]_{\psi} + \frac{\omega}{\rho} + \frac{p\rho_{\psi}}{\rho^2} = 0 \tag{2.1.25c}$$

$$\omega = \frac{1}{W}\left[\left(\frac{F}{\rho W}\right)_{\phi} - \left(\frac{E}{\rho W}\right)_{\psi}\right] \tag{2.1.25d}$$

$$K = \frac{1}{W}\left[\left(\frac{W}{E}\Gamma_{11}^2\right)_{\psi} - \left(\frac{W}{E}\Gamma_{12}^2\right)_{\phi}\right] = 0 \quad . \tag{2.1.25e}$$

Since the present work is concerned with the study of flow over airfoils, we need to know where the leading and trailing edges are mapped in the (ϕ,ψ) system. It is not possible to get exact values of ϕ at the leading and trailing

edges in (ϕ,ψ) system analytically. However, in general, these values can be obtained numerically by solving the equation

$$x_{\phi\phi} + x_{\psi\psi} = (E^{1/2}\cos\beta)_{\phi} + \left[\frac{F}{E^{1/2}}\cos\beta - \frac{J}{E^{1/2}}\sin\beta\right] ,$$

along with the flow equations, throughout the entire flow field (with appropriate conditions) such that

$$\beta_{\phi} = \frac{J}{E}\Gamma_{11}^2 ,$$

$$\beta_{\psi} = \frac{J}{E}\Gamma_{12}^2 ,$$

and $\tan\beta = y_{\phi}/x_{\phi}$, are satisfied.

2.2 von MISES TRANSFORMATION

Grossman and Barron [23], during the study of inviscid, incompressible flows, found that for an orthogonal system (i.e., F=0) the values of ϕ at leading and trailing edges cannot be obtained accurately and this causes inaccuracy in the solution near the leading and trailing edges.

To overcome this problem, Barron [24] has studied incompressible potential flow using a von Mises transformation defined by

$$x = \phi , \quad y = y(\phi,\psi) . \tag{2.2.1}$$

This transformation provides the exact locations of the

leading and trailing edges since the value of x at LE and TE are known. Since the coordinates ϕ,ψ satisfy the Gauss equation (2.1.25e) in order to form a curvilinear net, the von Mises transformation also must satisfy it so as to form a curvilinear net (x,ψ). It is easily verified that the transformation (2.2.1) identically satisfies (2.1.25e).

Applying the von Mises transformation to the system of equations (2.1.25), we get the following system of equations in the (x,ψ) system,

$$\sqrt{E} = \rho VW \tag{2.2.2a}$$

$$\left[\frac{V^2}{2} + \frac{p}{\rho}\right]_x + \frac{p\rho_x}{\rho^2} = 0 \tag{2.2.2b}$$

$$\left[\frac{V^2}{2} + \frac{p}{\rho}\right]_\psi + \frac{\omega}{\rho} + \frac{p}{\rho^2}\rho_\psi = 0 \tag{2.2.2c}$$

$$\omega = \frac{1}{W}\left[\left(\frac{F}{\rho W}\right)_x - \left(\frac{E}{\rho W}\right)_\psi\right] \tag{2.2.2d}$$

where

$$E = 1 + y_x^2$$

$$W = y_\psi$$

$$F = y_x y_\psi \quad .$$

The above system of equations serves as the starting point for the numerical work which follows.

CHAPTER III

NON-LIFTING PROBLEMS

In this chapter the flow equations (2.2.2) with appropriate boundary conditions are solved for steady, inviscid, irrotational, compressible flow over symmetric profiles at zero angle of attack. Solutions are obtained on non-stretched as well as stretched grids. Numerical algorithms are developed which are suitable for any high-speed computer. These algorithms have been tested on an IBM 4381-3 and results are presented which are in good agreement with the results of other researchers. All these algorithms involve inversion of large tridiagonal matrices.

As mentioned in the introduction, we are interested in that class of transonic flows for which the flow is isentropic and therefore the state equation in non-dimensional form is

$$p = \frac{\rho^{\gamma}}{\gamma M_{\infty}^{2}} , \quad M_{\infty} = \frac{u_{\infty}}{a_{\infty}}$$

where γ is the adiabatic constant and M_{∞}, a_{∞} are the free stream Mach number and speed of sound at infinity, respectively. For air γ has a value of 1.4.

3.1 BOUNDARY CONDITIONS

In order to have a well-posed boundary value problem, we have to add to equations (2.2.2) appropriate boundary conditions. Assuming a symmetric profile, we let

$$y = f(x) \qquad \text{-(3.1.1)}$$

be the equation of the profile and assume that the flow is uniform in the far field, parallel to the chord of the airfoil.

In the physical plane, the appropriate boundary conditions are

(i) $\rho = 1$, $u = 1$, $v = 0$ at infinity (3.1.2a)

(ii) tangency condition on the airfoil and symmetry:

$$\frac{v}{u} = \begin{cases} f'(x) & \text{on } y=f(x),\ x_{LE} \le x \le x_{TE} \\ 0 & \text{on } y=0,\ x<x_{LE} \text{ or } x>x_{TE} \end{cases} \qquad (3.1.2b)$$

where prime represents derivative with respect to "x".

These conditions are conveniently expressed in the (x,ψ) system by referring to the airfoil surface as a segment of the streamline $\psi = 0$. We have

(i) $\rho = 1$, $y = \psi$ at infinity (3.1.3a)

(ii) $$y=\begin{cases} f(x) & \text{on } \psi=0,\ x_{LE}\le x\le x_{TE} \\ 0 & \text{on } \psi=0,\ -\infty<x<x_{LE} \text{ or } x_{TE}<x<\infty \end{cases} \qquad (3.1.3b)$$

Now, using the state equation

$$p = \frac{\rho^{\gamma}}{\gamma M_\infty^2} \qquad (3.1.4)$$

in equations (2.2.2b,2.2.2c) and integrating and evaluating the constant of integration by applying (3.1.3a), we obtain

$$V^2 + \frac{2\rho^{\gamma-1}}{(\gamma-1)M_\infty^2} = 1 + \frac{2}{(\gamma-1)M_\infty^2} \qquad (3.1.5)$$

which is the Bernoulli's equation for steady, inviscid, irrotational, isentroptic, compressible fluid flow.

Employing (2.2.2a) in (3.1.5) we get

$$\frac{1+y_x^2}{\rho^2 y_\psi^2} + \frac{2\rho^{\gamma-1}}{(\gamma-1)M_\infty^2} = 1 + \frac{2}{(\gamma-1)M_\infty^2} \qquad (3.1.6)$$

The irrotionality condition is obtained from (2.2.2d) with $\omega=0$. Expanding this equation, we get the following well posed boundary value problem

$$y_\psi^2 y_{xx} - 2y_\psi y_x y_{\psi x} + (1+y_x^2) y_{\psi\psi} = \frac{y_x y_\psi^2 \rho_x}{\rho} - \frac{y_\psi (1+y_x^2)\rho_\psi}{\rho} \quad \text{(irrotationality)} \qquad (3.1.7a)$$

$$\frac{2\rho^{\gamma-1}}{(\gamma-1)M_\infty^2} + \frac{1+y_x^2}{\rho^2 y_\psi^2} = 1 + \frac{2}{(\gamma-1)M_\infty^2} \quad \text{(Bernoulli's equation)} \qquad (3.1.7b)$$

satisfying the conditions

$$\text{(i)}\quad \rho = 1 \quad \text{at infinity}$$
$$y = \psi \qquad\qquad (3.1.7c)$$

$$\text{(ii)}\quad y = \begin{cases} f(x) & \text{on } \psi = 0,\ x_{LE} \le x \le x_{TE} \\ 0 & \text{on } \psi = 0,\ -\infty < x < x_{LE} \text{ OR } x_{TE} < x < \infty \end{cases} . \qquad (3.1.7d)$$

It should be noted that in this new formulation the mixed type boundary value problem in the physical plane becomes a Dirichlet boundary value problem in the computational plane.

The Bernoulli's equation (3.1.7b) can be rewritten as

$$\rho = \left[1 - \frac{(\gamma-1)M_\infty^2}{2}\left(\frac{1+y_x^2}{\rho^2 y_\psi^2} - 1\right)\right]^{\frac{1}{\gamma-1}} . \qquad (3.1.8)$$

This equation indicates that there are two values of the density for a certain mass flux less than the maximum value which can be attained. For pure subsonic or supersonic flows one can easily decide which value to choose depending upon whether ρ is larger or smaller than ρ^*, the value of density at $a=a^*$, respectively. For mixed flow it is not obvious which value to choose.

Murman and Cole [11] were the first to introduce the idea of using central difference formulas in the subsonic zone and upwind formulas in the supersonic zone to account for the changing characteristics of the flow equations.

Jameson extended Murman's scheme [25] for full potential equations and developed highly sophisticated schemes such as the rotated difference scheme [26], fully conservative scheme [27]. etc. Researchers have also developed artificial viscosity and artificial compressibility methods [28-30] to overcome the problem mentioned in the previous paragraph. Jameson [29] modified density in the supersonic region by introducing an artifical viscosity term which vanishes in subsonic regions. The way in which he introduced the artificial viscosity term is briefly described here.

For a two-dimensional flow, the velocity potential ϕ satisfies the equation (using dimensional variables, but omitting the bars)

$$(a^2-u^2)\phi_{xx} - 2uv\,\phi_{xy} + (a^2-v^2)\phi_{yy} = 0$$

where u,v and "a" are the components of the velocity and the local speed of sound, respectively. If s and n denote the local streamwise and normal directions, then the above equation can be written in the form

$$(a^2-q^2)\phi_{ss} + a^2\,\phi_{nn} = 0$$

where

$$\phi_{ss} = (u^2\phi_{xx} + 2uv\,\phi_{xy} + v^2\phi_{yy})/q^2$$

$$\phi_{nn} = (v^2\phi_{xx} - 2uv\,\phi_{xy} + u^2\phi_{yy})/q^2$$

$$q^2 = u^2 + v^2 .$$

To introduce an artificial viscosity term in the supersonic region, Jameson used upwind difference formulas for derivatives contributing to ϕ_{ss}. The upwind difference formulas can be regarded as approximations to $\phi_{xx}-\phi_{xxx}\Delta x$, $\phi_{xy}-(\frac{\Delta x}{2})\phi_{xxy} - (\frac{\Delta y}{2})\phi_{xyy}$ and $\phi_{yy}-\phi_{yyy}\Delta y$. Thus, at supersonic points the artificial viscosity introduced is

$$(1-a^2/q^2)[\Delta x(u^2u_{xx} + uvv_{xx}) + \Delta y(uvu_{yy} + v^2v_{yy})] .$$

Jameson, in his formulation [29], obtained an equivalent form given by

$$-(\mu|u|\Delta x\rho_x)_x - (\mu|v|\Delta y\rho_y)_y$$

where

$$\mu = \max\ (0,1-a^2/q^2)$$

and hence, the modified density $\tilde{\rho}$ is defined by

$$\tilde{\rho} = \rho + \mu(\rho/a^2)(uu_x\Delta x + vv_y\Delta y).$$

The artificial compressibility method is based on the modified equation of continuity [30]

$$(\rho_1\phi_x)_x + (\rho_1\phi_y)_y = 0$$

where

$$\rho_1 = [1- \frac{M_\infty^2(\gamma-1)}{2}(\phi_x^2 + \phi_y^2 - \varepsilon(uf_x + vg_y)-1)]^{1/(\gamma-1)} .$$

The term $\varepsilon(uf_x+vg_y)$ is called the artificial viscosity

term. The form and magnitude of the viscous term is determined by numerical stability requirements.

In a manner similar to one described previously the density is also modified in the streamfunction formulation [30].

In our calculations, we employ an expression for modified density similar to that obtained by Hafez, Murman and South [30]. The expression for the modified density is taken as

$$\tilde{\rho} = \rho - (\mu \rho_x \Delta x) \tag{3.1.9}$$

where μ is the switching function which vanishes in subsonic regions and is defined by

$$\mu = \max\left(0,\ 1 - \frac{1}{M^2}\right)$$

where M is local Mach number.

3.2 NUMERICAL ALGORITHM

To solve the problem numerically, we must construct an appropriate set of difference equations. A grid is constructed so that the solution of the flow equations at the nodes gives a reasonable flow representation. In the present method the grid system has streamlines as one set of curves and ϕ=x as the second set of curves. The grid points are considered as ordered pairs (i,j), where i denotes the x-direction and j denotes the ψ-direction. The step sizes for the x and ψ directions, respectively, are

$$\Delta x = \frac{x_{max}-x_{min}}{i_{max}-i_{min}}, \quad \Delta\psi = \frac{\psi_{max}-\psi_{min}}{j_{max}-j_{min}}$$

where

x_{max} = value of x at i_{max}

x_{min} = value of x at i_{min}

etc.

Equation (3.1.7a) is discretized by using central differencing for all derivatives everywhere. This leads to a large system of non-linear algebraic equations in unknown "y" at the grid points. The finite difference approximation of equation (3.1.7a) at an (i,j) grid point is

$$a_1(y_{i+1j} - 2y_{ij} + y_{i-1j})$$

$$+ a_2(y_{i+1j+1} + y_{i-1j-1} - y_{i-1j+1} - y_{i+1j-1})$$

$$+ a_3(y_{ij+1} - 2y_{ij} + y_{ij-1})$$

$$= a_4\frac{(\tilde{\rho}_{i+1j}-\tilde{\rho}_{i-1j})}{\tilde{\rho}_{ij}} + a_5\frac{(\tilde{\rho}_{ij+1}-\tilde{\rho}_{ij-1})}{\tilde{\rho}_{ij}} \qquad (3.2.1)$$

where $\tilde{\rho}$ is the modified density. The coefficients in (3.2.1) are

$$a_1 = \left(\frac{y_{ij+1}-y_{ij-1}}{2\,\Delta\psi}\right)^2$$

$$a_2 = \frac{-2\Delta x^2(y_{ij+1}-y_{ij-1})(y_{i+1j}-y_{i-1j})}{(4\Delta x\Delta\psi)(4\Delta x\Delta\psi)}$$

$$a_3 = \frac{\Delta x^2}{\Delta \psi^2}\left(1 + \left(\frac{y_{i+1j} - y_{i-1j}}{2\Delta x}\right)^2\right)$$

$$a_4 = \frac{\Delta x^2 (y_{i+1j} - y_{i-1j})(y_{ij+1} - y_{ij-1})^2}{(4\Delta x \Delta \psi)^2}$$

$$a_5 = \frac{-\Delta x^2 (y_{ij+1} - y_{ij-1})}{(2\Delta\psi)(2\Delta\psi)}\left(1 + \left(\frac{y_{i+1j} - y_{i-1j}}{2\Delta x}\right)^2\right)$$

$$\tilde{\rho}_{ij} = \rho_{ij} - \mu_{ij}(\rho_x \Delta x)_{ij}$$

$$\rho_{ij} = \left[1 + \frac{(\gamma-1)M_\infty^2}{2} - \frac{(\gamma-1)M_\infty^2}{2} a_6\right]^{1/\gamma - 1}$$

$$a_6 = \frac{\left[1 + \left(\frac{y_{i+1j} - y_{i-1j}}{2\Delta x}\right)^2\right](2\Delta\psi)^2}{\tilde{\rho}_{ij}^2 (y_{ij+1} - y_{ij-1})^2}$$

and

$$\mu_{ij} = \max\left(0,\ 1 - \frac{1}{M_{ij}^2}\right) .$$

Equation (3.2.1) in the matrix form can be written as

$$N\bar{S} = \bar{H} \qquad (3.2.3)$$

where N, $\bar{S}$, $\bar{H}$, are, respectively (i-2)*(j-2), (j-2)*1, (i-2)*1 matrices. The elements of $\bar{S}$ consist of the function y for each point in the computation domain, and the vector $\bar{H}$ contains specified boundary values. The matrices in (3.2.3) are

$$N = \left[\right.$$

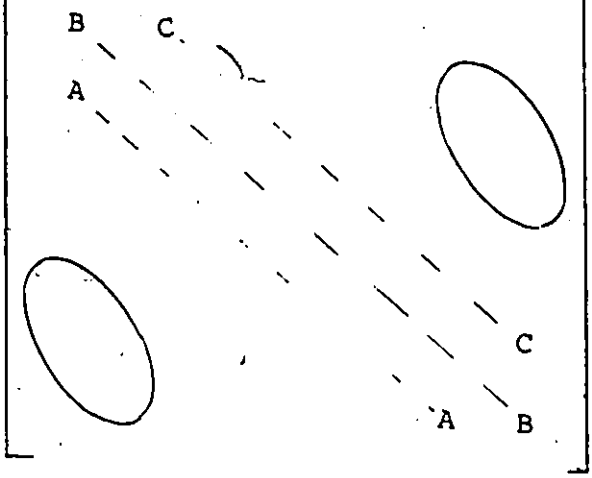

$$\left. \right]$$

$$\bar{S} = \begin{bmatrix} \vec{y}_2 \\ \vec{y}_3 \\ \vdots \\ \vec{y}_{i_{max-1}} \end{bmatrix}$$

$$\bar{H} = \begin{bmatrix}
- a_1 y_{12} - a_3 y_{21} - a_2(y_{11} - y_{13} - y_{31}) + Q(2,2) \\
- a_1 y_{13} - a_2(y_{12} - y_{14}) + Q(2,3) \\
\vdots \\
- a_1 y_{1 j_{max-2}} - a_2(y_{1 j_{max-3}} - y_{1 j_{max-1}}) + Q(2, j_{max-2}) \\
- a_1 y_{1 j_{max-1}} - a_3 y_{2 j_{max}} - a_2(y_{3 j_{max}} + y_{1 j_{max-2}} - y_{1 j_{max}}) \\
\quad + Q(2, j_{max-1}) \\
\hline
- a_3 y_{31} - a_2(y_{21} - y_{41}) + Q(3,2) \\
Q(3,3) \\
Q(3,4) \\
\vdots \\
Q(3, j_{max-2}) \\
- a_3 y_{3 j_{max}} - a_2(y_{4 j_{max}} - y_{2 j_{max}}) + Q(3, j_{max-1}) \\
\hline
\vdots \\
\hline
-a_1 y_{i_{max} 2} - a_3 y_{i_{max-1} 1} - a_2(y_{i_{max} 3} - y_{i_{max} 1} \\
\quad + y_{i_{max-2} 1}) + Q(i_{max-1}, 2)
\end{bmatrix}$$

continued

$$\begin{bmatrix} - a_1 y_{i_{max}3} - a_2(y_{i_{max}4} - y_{i_{max}2}) + Q(i_{max-1}, 3) \\ \\ - a_1 y_{i_{max}j_{max-2}} - a_2(y_{i_{max}j_{max-1}} - y_{i_{max}j_{max-3}} \\ + Q(i_{max-1}, j_{max-2}) \\ -a_1 y_{i_{max}j_{max-1}} - a_3 y_{i_{max-1}j_{max}} - a_2(y_{i_{max}j_{max}} \\ - y_{i_{max-2}j_{max}} - y_{i_{max}j_{max-2}} + Q(i_{max-1}, j_{max-1}) \end{bmatrix}$$

where

$$Q(i,j) = \frac{a_4(\tilde{\rho}_{i+1j} - \tilde{\rho}_{i-ij})}{\tilde{\rho}_{ij}} + \frac{a_5(\tilde{\rho}_{ij+1} - \tilde{\rho}_{ij-1})}{\tilde{\rho}_{ij}}$$

$$\vec{y}_k = \begin{bmatrix} y_{k2} \\ y_{k3} \\ \vdots \\ y_{k,j_{max-1}} \end{bmatrix}, \quad k = 2,3\ldots, (i_{max-1})$$

and $A = \text{trid}\ (a_3, a_1+a_3, a_3)$

$B = \text{trid}\ (-a_2, a_1, a_2)$

$C = \text{trid}\ (a_2, a_1, -a_2)$.

In the whole flow region density ρ and modified density $\tilde{\rho}$ are computed using central differencing for derivatives y_x and y_ψ except along the line $\psi=0$. Along $\psi=0$, i.e., $j=1$, y_ψ and y_x are computed from

$$y_\psi\Big|_{i1} \doteq \frac{(y_{i2}-y_{i1})}{\Delta\psi} ,$$

$$y_x\Big|_{i1} = \begin{cases} f'(x_i) , & x_{LE}\leq x_i \leq x_{TE} \\ 0 , & -\infty<x_i<x_{LE} \text{ or } x_{TE}<x_i<\infty . \end{cases}$$

For speed calculations, differencing for derivatives is the same as used for ρ and $\tilde{\rho}$ except in the supersonic region where backward differencing is employed for y_x. The ρ and $\tilde{\rho}$ are, respectively, relaxed through relations

$$\rho_{ij}^{(n+1)} = (1-w_1)\rho_{ij}^{(n)} + w_1\left[1+\frac{(\gamma-1)M_\infty^2}{2} - \frac{(\gamma-1)M_\infty^2}{2}a_6^{(n)}\right]^{1/(\gamma-1)} \tag{3.2.4}$$

$$\tilde{\rho}_{ij}^{(n+1)} = (1-w_2)\tilde{\rho}_{ij}^{(n)} + w_2(\tilde{\rho}_{ij}^{(n)} - \mu_{ij}^{(n)}(\rho_x\Delta x)_{ij}^{(n)}) \tag{3.2.5}$$

where "n" is the iteration level and w_1, w_2 are relaxation parameters. The pressure coefficient is computed from

$$C_p = \frac{2(\tilde{\rho}^\gamma-1)}{\gamma M_\infty^2} . \tag{3.2.6}$$

SLOR, with sweep from left to right, is used to solve the system (3.2.3). A simple algorithm which solves (3.2.3) is

Step 1. Construct a computational domain with given grid size and grid spacing i.e., specify x_{max}, x_{min},..., etc.,

Step 2. Initialize ρ_{ij}, $\tilde{\rho}_{ij}$ to 1 for all i and j and set

$$y_{ij} = \psi_{min} + (j-1)\Delta\psi \quad \text{for all } j>1.$$

and

$$y_{il} = \begin{cases} f(x_i) & \text{for } i_{LE} \le i \le i_{TE} \\ 0 & \text{for } i<i_{LE} \text{ or } i>i_{TE}. \end{cases}$$

Step 3. Central difference all derivatives except y_ψ along j=1, where a two point forward differencing for y_ψ is used. Solve (3.2.3) for y in the whole computational domain, calculating the coefficients a_1, a_2, a_3 and Q(i,j) at the previous iteration level, until the error tolerance for y is met.

Step 4. Use values of $\tilde{\rho}$ and y (obtained from step 3) to calculate ρ from (3.1.8) and use this to calculate $\tilde{\rho}$ from (3.1.9).

Step 5. Check the convergence for ρ and $\tilde{\rho}$. Continue iteration until tolerance levels for y, ρ, $\tilde{\rho}$, are achieved.

This algorithm provides results which are in good agreement with the results of other researchers.

3.3 STRETCHING TRANSFORMATION

In the last section, we solved the flow equations with appropriate boundary conditions in un-stretched coordinates. In order to solve in the stretched coordinates, following Jones [31], we introduce transformations defined by

$$x = A \tan\xi \exp(-B\xi^2) \tag{3.3.1}$$

$$\psi = D \tan\eta \ . \tag{3.3.2}$$

These transformations transfer $x=\pm\infty$, $\psi=\pm\infty$ to $\xi=\pm\pi/2$ and $\eta=\pm\pi/2$, respectively. Another benefit of these transformations is that they provide us with a dense mesh in the vicinity of the airfoil. The former helps to make mesh points more dense near leading and trailing edges of the airfoil and the latter to pack more points near the x-axis with airfoil centered at x=0. The computational boundaries used for our purpose are

$$\begin{aligned} -\pi/2 + \varepsilon \leq \xi \leq \pi/2 - \varepsilon \\ -\pi/2 + \varepsilon \leq \eta \leq \pi/2 - \varepsilon \end{aligned} \tag{3.3.3}$$

and A,B,D, constants in the transformations, are kept constant at 0.9, 0.6, 0.4, respectively. The ε is chosen such that the above boundaries correspond to (x,ψ)-plane boundaries

$$\begin{aligned} -6.0 \leq x \leq 6.0 \\ 0 \leq \psi \leq 6.0 \ . \end{aligned} \tag{3.3.4}$$

Jones [31] has discussed in detail how the constants in transformations (3.3.1-3.3.2) are chosen.

3.4 TRANSFORMATION OF THE FULL POTENTIAL EQUATION IN STRETCHED COORDINATES

For general transformations of the type (3.3.1-3.3.2) we write

$$x = x(\xi), \quad \psi = \psi(\eta) \ . \tag{3.4.1}$$

For convenience in handling the boundary conditions at infinity, we introduce a new variable Y defined by

$$y = Y + \psi \ . \tag{3.4.2}$$

Using (3.4.2) in (3.1.7a), we obtain,

$$(1+Y_\psi)^2 Y_{xx} - 2Y_x(1+Y_\psi)Y_{\psi x} + (1+Y_x^2)Y_{\psi\psi}$$

$$= \frac{Y_x(1+Y_\psi)^2\tilde{\rho}_x}{\tilde{\rho}} - \frac{(1+Y_\psi)(1+Y_x^2)\tilde{\rho}_\psi}{\tilde{\rho}} \ . \tag{3.4.3}$$

Using transformation (3.4.1) in (3.4.3), we get,

$$A_1 Y_{\xi\xi} + A_2 Y_{\eta\eta} + A_3 Y_{\eta\xi} + A_4 Y_\xi + A_5 Y_\eta = \psi_\eta^2 x_\xi^2 A_6 \tag{3.4.4}$$

where

$$A_1 = [\psi_\eta + Y_\eta]^2$$

$$A_2 = [x_\xi^2 + Y_\xi^2]$$

$$A_3 = -2Y_\xi[Y_\eta + \psi_\eta]$$

$$A_4 = -[\psi_\eta + Y_\eta]^2 \frac{x_{\xi\xi}}{x_\xi}$$

$$A_5 = -[x_\xi^2 + y_\xi^2] \frac{\psi_{\eta\eta}}{\psi_\eta}$$

$$A_6 = \frac{Y_\xi[\psi_\eta + Y_\eta]^2\tilde{\rho}_\xi}{\tilde{\rho}} - \frac{[\psi_\eta + Y_\eta][x_\xi^2 + Y_\xi^2]\tilde{\rho}_\eta}{\tilde{\rho}}$$

The boundary conditions in the (ξ,η)-system are

$$Y = \begin{cases} f(\xi) & \text{for } \xi_{LE} \leq \xi \leq \xi_{TE} \\ 0 & \text{for } \xi < \xi_{LE} \text{ or } \xi > \xi_{TE} \end{cases}$$

$$\tilde{\rho} = \rho = 1 \quad \text{at } \infty$$

$$Y = 0 \quad \text{at } \infty$$

where ξ_{LE} and ξ_{TE} are the values of x_{LE} and x_{TE}, respectively, in the (ξ,η)-plane. Since the flow is symmetric about the ξ-axis, the computational domain is taken as

$$-\frac{\pi}{2} + \varepsilon \leq \xi \leq \frac{\pi}{2} - \varepsilon$$

$$0 \leq \eta \leq \frac{\pi}{2} - \varepsilon \ .$$

The differencing and solution algorithm are the same as that employed in the (x,ψ)-system. The finite difference representation of equation (3.4.4) at an (i,j) grid point is

$$A_1 \frac{[Y_{i+1j} - 2Y_{ij} + Y_{i-1j}]}{(\Delta\xi)^2}$$

$$+ A_2 \frac{[Y_{ij+1} - 2Y_{ij} + Y_{ij-1}]}{(\Delta\eta)^2}$$

$$+ A_3 \frac{[Y_{i+1j+1} + Y_{i-1j-1} - Y_{i-1j+1} - Y_{i+1j-1}]}{4\Delta\xi\Delta\eta}$$

$$+ A_4\left[\frac{Y_{i+1j} - Y_{i-1j}}{2\Delta\xi}\right] + A_5\left[\frac{Y_{ij+1} - Y_{ij-1}}{2\Delta\eta}\right]$$

$$= \frac{\psi_\eta^2 x_\xi^2}{\tilde{\rho}}\left\{\left[\frac{(y_{i+1j} - Y_{i-1j})}{2\Delta\xi}\right]\left[\psi_\eta + \frac{(Y_{ij+1} - Y_{ij-1})}{2\Delta\eta}\right]^2\right.$$

$$\left[\frac{\tilde{\rho}_{i+1j} - \tilde{\rho}_{i-1j}}{2\Delta\xi}\right]$$

$$- \left[\psi_\eta + \left(\frac{Y_{ij+1} - Y_{ij-1}}{2\Delta\eta}\right)\right]\left[x_\xi^2 + \left(\frac{Y_{i+ij} - Y_{i-1j}}{2\Delta\xi}\right)^2\right]$$

$$\left.\left[\frac{\tilde{\rho}_{ij+1} - \tilde{\rho}_{ij-1}}{2\Delta\eta}\right]\right\} \qquad (3.3.5)$$

where x_ξ, $x_{\xi\xi}$, ψ_η, $\psi_{\eta\eta}$ are calculated from (3.3.1-3.3.2).

In the matrix form (3.3.5) can be written as

$$T\bar{Y} = \bar{R} \qquad (3.3.6)$$

where

$$T = \begin{bmatrix} B & C & & & & \\ A & & & & & \\ & & & & & \\ & & & & & \\ & & & & C & \\ & & & & A & B \end{bmatrix}$$

and

$$A = \text{trid}\left(\frac{A_3\beta}{4},\ A_1 - \frac{A_4\Delta\xi}{2},\ -\frac{A_3\beta}{4}\right)$$

$$B = \text{trid}\left(A_2\beta^2 - \frac{A_5\Delta\xi\beta}{2},\ -2(A_1+A_2\beta^2),\ A_2\beta^2 + \frac{A_5\Delta\xi\beta}{2}\right)$$

$$C = \text{trid}\left(-\frac{A_3\beta}{4},\ A_1 + \frac{A_4\Delta\xi}{2},\ \frac{A_3\beta}{4}\right)$$

$$\beta = \frac{\Delta\xi}{\Delta\eta}$$

$$\bar{Y} = \begin{bmatrix} \vec{Y}_1 \\ \vec{Y}_2 \\ \\ \vec{Y}_{i_{max-1}} \end{bmatrix}, \quad \vec{Y}_K = \begin{bmatrix} Y_{K2} \\ Y_{K3} \\ \\ Y_{Kj_{max-1}} \end{bmatrix}, \quad K=2,3,\ldots,\ i_{max-1}$$

$$\bar{R} = \begin{bmatrix} -(A_1 - \frac{A_4\Delta\xi}{2})Y_{12} - (A_2\beta^2 - \frac{A_5\Delta\xi\beta}{2})Y_{21} - \frac{A_3\beta}{4} \\ (Y_{11}-Y_{13}-Y_{31}) + H_1(2,2) \\ -(A_1 - \frac{A_4\Delta\xi}{2})Y_{13} - \frac{A_3\beta}{4}(Y_{12}-Y_{14}) + H_1(2,3) \\ \\ -(A_2\beta^2 + \frac{A_5\Delta\xi\beta}{2})\ Y_{2j_{max}} + (A_2\beta^2 - \frac{A_5\Delta\xi\beta}{2})Y_{1j_{max-2}} \\ -\frac{A_3\beta}{4}(Y_{3j_{max}} + Y_{1j_{max-2}} + Y_{1j_{max}}) + H_1(2,j_{max-1}) \end{bmatrix}$$

Continued

$$
\begin{bmatrix}
-(A_2\beta^2 - \frac{A_5\Delta\xi\beta}{2})Y_{31} - \frac{A_3\beta}{4}(Y_{21}-Y_{41}) + H_1(3,2) & & \\
 & H_1(3,3) & \\
 & \vdots & \\
 & H_1(3,j_{max-2}) & \\
-(A_2\beta^2 + \frac{A_5\Delta\xi\beta}{2})Y_{3j_{max}} - \frac{A_3}{4}(Y_{4j_{max}}) + H_1(3,j_{max-1}) & & \\
\hline
 & \vdots & \\
\hline
-(A_1 + \frac{A_4\Delta\xi}{2})Y_{i_{max}2} - (A_2\beta^2 - \frac{A_5\Delta\xi\beta}{2})Y_{i_{max-1}1} & & \\
\frac{A_3\beta}{4}(Y_{i_{max-2}1} - Y_{i_{max}1} + Y_{i_{max}3}) + H_1(i_{max-1},2) & & \\
 & \vdots & \\
-(A_1 + \frac{A_4\Delta\xi}{2})Y_{i_{max}j_{max-1}} - (A_2\beta^2 + \frac{A_5\Delta\xi\beta}{2})Y_{i_{max-1}j_{max}} & & \\
-\frac{A_3\beta}{4}(Y_{i_{max}j_{max}} - Y_{i_{max-2}j_{max}} - Y_{i_{max}j_{max-2}}) & & \\
+ H_1(i_{max-1}, j_{max-1}) & &
\end{bmatrix}
$$

where

$$H_1(i,j) = A_6\psi_\eta^2(j)x_\xi^2(i)(\Delta\xi)^2.$$

3.5 FINE GRID SOLUTIONS

During the study in the previous section, it was found that y fails to converge on finer grids. This was possibly due to the freezing of the terms involving density derivatives and also, perhaps, the use of the artificial compressibility method. To achieve convergence on a fine grid it was necessary to have irrotationality condition independent of ρ_x and ρ_ψ and avoid the use of artificial density which introduces a numerical error in the solution, as indicated by [32]. To accomplish this, the momentum equations(2.2.2b, 2.2.2c) were used to eliminate ρ_x and ρ_ψ from equation(3.1.7a) yielding equation

$$(y_\psi^2 - \frac{M_\infty^2}{\rho^{\gamma+1}})y_{xx} - 2y_x y_\psi y_{x\psi} + (1+y_x^2)y_{\psi\psi} = 0 \qquad (3.5.1)$$

In (ξ,η)-system equation (3.5.1) becomes

$$A_1 y_{\xi\xi} + A_2 y_{\eta\eta} + A_2 y_{\xi\eta} + A_4 y_\xi + A_5 y_\eta = 0 \qquad (3.5.2)$$

where

$$A_1 = (\psi_\eta + y_\eta)^2 - \frac{M_\infty^2 \psi_\eta^2}{\rho^{\gamma+1}}$$

$$A_2 = x_\xi^2 + y_\xi^2$$

$$A_3 = -2y_\xi(\xi_\eta + y_\eta)$$

$$A_4 = -A_1 x_{\xi\xi}/x_\xi$$

$$A_5 = -A_2 \psi_{\eta\eta}/\psi_\eta$$

This equation is of elliptic, parabolic or hyperbolic type, in accordance with the value of local Mach number being less than, equal to, or greater than 1. Equation (3.5.2) has been solved in a fine grid using type dependent differencing and solutions obtained are presented in the next section.

3.6 RESULTS AND DISCUSSION

The algorithm described in section 3.2 has been used to compute full-potential subcritical and supercritical flows over a NACA 0012 airfoil and a 6% circular arc airfoil. Results have been obtained on both uniform and stretched grids.

Figure(2)gives the pressure distribution on a NACA 0012 airfoil at M =0.63. Comparison is made with the results of Garabedian and Korn [14], Sinclair's field panel method [33] and the panel method [33]. Our calculation on the stretched grid agrees very well with previous results [14, 33]. Our results on the un-stretched grid show some difference near the trailing edge. However, these results have been computed on a 70x36 grid, yielding only 8 grid points on the airfoil surface. Our results are excellent

considering that Sinclair has used 50 surface points to achieve this solution.

The pressure coefficient on the streamline $\psi=0$ for the NACA 0012 airfoil at $M_\infty=0.7$ is illustrated in Figure (3). Comparison with the results of Hafez and Lovell [19] for this subcritical flow shows that the present method predicts C_p very accurately, particularly on the stretched grid.

A supercritical flow at $M_\infty=0.8$ on the NACA 0012 airfoil was computed and is compared with results of Garabedian and Korn [14] and Sinclair [33] in Figure (4). Here the stretched grid results show excellent agreement with earlier work.

In the calculation of transonic supercritical flows using artificial compressibility methods, the switching parameter μ can be used to control the amount of artificial compressibility added to the flow. The value of μ at each grid point is determined from $\mu_{ij} = \max(0, 1-\frac{1}{M_{ij}^2})$ but can be adjusted by a multiplicative factor to improve the convergence. Also, it is well known that difficulties occur in the calculation of ρ from (3.1.8) when the grid is refined. One way to control these difficulties is to increase the amount of artificial compressibility as the number of grid points increases. This idea is illustrated in Figure (5) where C_p's for the NACA 0012 airfoil at $M_\infty=0.8$ is compared on grid 49 x 16. To control the density

growth in the supersonic region we have taken $\mu_{ij}=C\max(0,1-\frac{1}{M_{ij}^2})$ and allowed C to increase as the grid spacing is decreased.

The pressure distribution on a 6% circular arc airfoil at $M_\infty=0.817$ is compared with experimental measurements due to Earl [35] in Figure 6. Agreement is good for this subcritical flow and improves much on the stretched grid.

Several parameters have been fixed in the programmes. After some numerical experimentation it was found that the best choice for the relaxation parameters was $w_1=.7$ and $w_2=.5$, respectively. The constants A, B and D appearing in the stretching functions (3.3.1) and (3.3.2) are kept constant at 0.9, 0.6 and 0.4, respectively. These values have been chosen to provide accurate solutions by controlling the degree of clustering and to accelerate the convergence of the iterative process. Tables 1 and 2 summarize the computational information for the NACA 0012 and 6% circular arc airfoils, giving the number of iterations and CPU times for various Mach numbers and grid sizes. The savings in CPU time by using the stretched grid is clearly evident. It should also be pointed out that the CPU times provided are based on calculations performed on an IBM 4381-3 under WATFIV JCL. These times can be reduced by a factor of about 1/3 by using FORTRAN

JCL. Finally, in all cases a tolerance level of 10^{-4} was used for the convergence under the maximum norm. The convergence history for the density is shown in Figure (6).

Results are computed using equation (3.5.2) for subcritical and supercritical flows on the NACA 0012 and 6% circular arc airfoils on finer grids at different Mach numbers. To avoid drastic change in the density between iterations in the supersonic region we adopted the following strategy.

After updating the density, we ensured that the new density did not drop by more than Δx% of the minimum of the three densities $\rho_{i-1j}^{(n+1)}$, $\rho_{ij}^{(n)}$, $\rho_{i+1j}^{(n)}$ or exceed by more than Δx% of the maximum of the densities $\rho_{i-1j}^{(n+1)}$, $\rho_{ij}^{(n)}$, $\rho_{i+1j}^{(n)}$. A similar strategy has also been used successfully by Wigton [34]. In fact, Wigton points out very clearly the difficulties in obtaining fine grid solutions and is only able to achieve convergence through this strategy.

Figures (8 - 11) show the plot of C_p calculated on the NACA 0012 and 6% circular arc airfoils for subcritical and supercritical flows. As indicated on these figures and in Table 3 convergence has been obtained in very fine grids, yielding as many as 70 surface points on a NACA 0012 at $M_\infty=0.7$.

Figure (12) shows the convergence of y against

the number of iterations. Further information on grid sizes, number of iterations and CPU times are given in Table 3.

CHAPTER IV

INVERSE PROBLEMS

In Chapter III we solved the direct problem, i.e., problems in which the geometry of the body was prescribed and the flow field was computed subject to appropriate boundary conditions. In this chapter we study inverse or design problems. In the inverse problem the objective is to determine the body geometry corresponding to a given distribution of surface pressure or velocity. The inverse problem has received less attention in the literature as compared to the direct problem. Recent development of new airfoils suitable for future transport aircraft cruising at high subsonic Mach numbers has attracted the attention of researchers to the inverse problem. For an aircraft designer the solution to inverse problems are much more useful in designing optimum aerodynamic shapes, since he can input a pressure or velocity distribution that is known to have desirable features and then obtain the corresponding body shape. In this way one can save considerable time and effort as compared to the alternative approach, which is to solve the direct problem for a number

of shapes and then choose the one that produces the desired features [37-39].

In this chapter, a method for solving the inverse problem is developed which is simple, fast, and provides results in excellent agreement with the original shapes.

4.1 FLOW EQUATIONS AND BOUNDARY CONDITIONS

The equations governing an inviscid, irrotational, isentropic compressible fluid flow, in the (x,ψ) - plane, are

$$y_\psi^2 y_{xx} - 2y_\psi y_x y_{x\psi} + (1+y_x^2) y_{\psi\psi} = \frac{y_\psi^2\, y_x \rho_x}{\rho} - \frac{y_\psi (1+y_x^2)\rho_\psi}{\rho} \quad \text{(irrotationality)} \tag{4.1.1}$$

$$\frac{2\rho^{\gamma-1}}{(\gamma-1)M_\infty^2} + \frac{1+y_x^2}{\rho^2 y_\psi^2} = 1 + \frac{2}{(\gamma-1)M_\infty^2}. \quad \text{(Bernoulli's equation)} \tag{4.1.2}$$

The pressure coefficient C_p is given by

$$C_p = \frac{2(\rho^\gamma - 1)}{\gamma M_\infty^2} . \tag{4.1.3}$$

Without loss of generality, we choose the airfoil to be a segment of the streamline $\psi=0$. Since we prescribe the pressure distribution for the inverse problem, equation (4.1.3) is rearranged in the form

$$\rho = \left(1 + \frac{\gamma M_\infty^2}{2} C_p\right)^{1/\gamma} \quad \text{on } \psi = 0,\ x\in[x_{LE}, x_{TE}] \tag{4.1.4}$$

The Bernoullis' equation (4.1.2) gives

$$y_\psi = \sqrt{\frac{1+y_x^2}{\rho^2\left(1+\frac{2}{(\gamma-1)M_\infty^2}-\frac{2\rho^{\gamma-1}}{(\gamma-1)M_\infty^2}\right)}} \qquad (4.1.5)$$

The well-posed boundary value problem for airfoil design is to solve

$$y_\psi^2 y_{xx} - 2y_\psi y_x y_{x\psi} + (1+y_x^2)y_{\psi\psi}$$

$$= \frac{y_\psi^2 y_x \rho_x}{\rho} - \frac{y_\psi(1+y_x^2)\,\rho_\psi}{\rho} \quad \text{for } \psi>0 \qquad (4.1.6a)$$

with

$$y_\psi = b\sqrt{1+y_x^2} \quad \text{on } \psi = 0,\ x_{LE}\le x\le x_{TE} \qquad (4.1.6b)$$

$$\rho = \begin{cases} \left(1+\frac{\gamma M_\infty^2}{2}C_p\right)^{1/\gamma} & \text{on } \psi = 0,\ x_{LE}\le x\le x_{TE} \\ 1 & \text{at } \infty \end{cases} \qquad (4.1.6c)$$

$$y = 0 \quad \text{on } \psi = 0,\ -\infty<x<x_{LE} \quad \text{or} \quad x_{TE}<x<\infty$$

$$y = \psi \quad \text{at } \infty \qquad (4.1.6d)$$

where

$$b = \frac{1}{\sqrt{a_1^2\left(1+\frac{2}{(\gamma-1)M_\infty^2}-\frac{2a_1^{\gamma-1}}{(\gamma-1)M_\infty^2}\right)}}$$

$$a_1 = \left(1+\frac{\gamma M_\infty^2}{2}C_p\right)^{1/\gamma} \qquad (4.1.6e)$$

along with (4.1.2).

On introducing modified density $\tilde{\rho}$, the system (4.1.6) is replaced by the following new system:

$$y_\psi^2 y_{xx} - 2y_\psi y_x y_{x\psi} + (1+y_x^2) y_{\psi\psi}$$

$$= \frac{y_\psi^2 y_x \tilde{\rho}_x}{\tilde{\rho}} - \frac{y_\psi (1+y_x^2) \tilde{\rho}_\psi}{\tilde{\rho}} \qquad \text{for } \psi>0 \qquad (4.1.7a)$$

$$y_\psi = b\sqrt{1 + y_x^2} \qquad \text{on } \psi=0,\ x_{LE} \le x \le x_{TE} \qquad (4.1.7b)$$

$$\tilde{\rho} = \begin{cases} (1 + \frac{\gamma M_\infty^2}{2} C_p)^{1/\gamma} & \text{on } \psi=0,\ x_{LE} \le x \le x_{TE} \\ 1 & \text{at } \infty \end{cases} \qquad (4.1.7c)$$

$$y = \psi \qquad \text{at } \infty$$

$$y = 0 \qquad \text{on } \psi=0;\ -\infty<x<x_{LE} \text{ or } x_{TE}<x<\infty \qquad (4.1.7d)$$

along with equation (4.1.2) and where b is given by (4.1.6e).

4.2 NUMERICAL ALGORITHM FOR UN-STRETCHED GRIDS

The equation (4.1.7a) is discretized by using central differencing for all derivatives everywhere except on $\psi = 0$ for $x_{LE} \le x \le x_{TE}$. Considering the grid points as ordered pairs (i,j), the finite difference approximation of equation (4.1.7a) at an (i,j) grid point can be written as

$$C_1(y_{i+1j} - 2y_{ij} + y_{i-1j})$$

$$+C_2(y_{i+1j+1} + y_{i-1j-1} - y_{i-1j+1} - y_{i+1j-1})$$

$$+ C_3(y_{ij+1} - 2y_{ij} + y_{ij-1})$$

$$= [C_4(\tilde{\rho}_{i+1j} - \tilde{\rho}_{i-1j}) + C_5(\tilde{\rho}_{ij+1} - \tilde{\rho}_{ij-1})]/\tilde{\rho}_{ij} \qquad (4.2.1)$$

where

$$C_1 = \left(\frac{y_{ij+1} - y_{ij-1}}{2\Delta\psi}\right)^2$$

$$C_2 = \frac{2\Delta x^2(y_{ij+1} - y_{ij-1})(y_{i+1j} - y_{i-1j})}{(4\Delta x\Delta\psi)^2}$$

$$C_3 = \frac{\Delta x^2}{\Delta\psi^2}\left[1 + \left(\frac{y_{i+1j} - y_{i-1j}}{2\Delta x}\right)^2\right]$$

$$C_4 = \frac{\Delta x^2(y_{i+1j} - y_{i-1j})(y_{ij+1} - y_{ij-1})^2}{2\Delta x(2\Delta\psi)^2(2\Delta x)}$$

$$C_5 = -\Delta x^2\frac{(y_{ij+1} - y_{ij-1})}{(2\Delta\psi)(2\Delta\psi)}\left(1 + \left(\frac{y_{i+1j} - y_{i-1j}}{2\Delta x}\right)^2\right)$$

$$\tilde{\rho}_{ij} = \rho_{ij} - \mu_{ij}(\rho_x\Delta x)_{ij}$$

$$\rho_{ij} = \left[1 + \frac{(\gamma-1)M_\infty^2}{2} - \frac{(\gamma-1)M_\infty^2 a_6}{2}\right]^{1/(\gamma-1)}$$

$$a_6 = \frac{(2\Delta\psi)^2\left[1 + \left(\frac{y_{i+1j} - y_{i-1j}}{2\Delta x}\right)^2\right]}{\tilde{\rho}_{ij}^2(y_{ij+1} - y_{ij-1})^2}$$

$$\mu_{ij} = \max\left(0, 1 - \frac{1}{M_{ij}^2}\right) .$$

On $\psi=0$, $x_{LE} \leq x \leq x_{TE}$ the equation (4.1.7b) is discretized as follows:

Along $\psi=0$, $x_{LE} \leq x \leq x_{TE}$, on using (4.1.7b) and (4.1.2)

in (4.1.7a), we get,

$$A^* y_{xx} + B^* y_{\psi\psi} = C^*$$

where

$$A^* = \frac{1-y_x^2}{G}$$

$$B^* = 1+y_x^2$$

$$C^* = -y_x(1+y_x^2)K(\rho)\rho_x - \frac{(1+y_x^2)^{3/2}}{\rho\sqrt{G}}\rho_\psi$$

$$G = \rho^2[a_1^*+b^*\rho^{\gamma-1}]$$

$$K(\rho) = (A^*+b^*\gamma\rho^{\gamma-1})\rho/G^2$$

$$a_1^* = 1+\frac{2}{(\gamma+1)M_\infty^2}$$

$$b^* = \frac{2}{(\gamma-1)M_\infty^2} .$$

Employing, along j=1, the approximations

$$y_{\psi\psi} \doteq \frac{2(y_{i2}-y_{i1})}{\Delta\psi^2} - \frac{2}{\Delta\psi}(y_\psi)_{j=1}$$

$$y_x \doteq \frac{(y_{i+1\ 1} - y_{i-1\ 1})}{2\Delta x}$$

$$y_{xx} \doteq \frac{(y_{i+1\ 1} - 2y_{i1}+y_{i-1\ 1})}{\Delta x^2} ,$$

the above equation gives

$$A^*[y_{i+1\ 1} - 2y_{i1} + y_{i-1\ 1}] + B^*[2\beta^2(y_{i2}-y_{i1}) - 2\beta\Delta x(y_{\psi})_{j=1}] = C^*(\Delta x)^2 \qquad (4.2.2)$$

where

$$\beta = (\Delta x/\Delta\psi) .$$

The matrix representation of (4.2.1) is the same as (3.2.3).

Equation (4.2.2) provides tridiagonal elements along $\psi=0$, $x_{LE} \leq x \leq x_{TE}$, which are

$$A(1) = 0$$

$$B(1) = 2d_1 - 2d_2$$

$$C(1) = 2d_2$$

$$RHS(1) = -d_1(y_{i+1\ 1} + y_{i-1\ 1}) + d_3 + d_4$$

where

$$d_1 = \frac{1-(\frac{y_{i+1\ 1}-y_{i-1\ 1}}{2\Delta x})^2}{d_5}$$

$$d_2 = [1+ \frac{(y_{i+1\ 1}-y_{i-1\ 1})^2}{2\Delta x}](\frac{\Delta x}{\Delta\psi})^2$$

$$d_3 = \frac{2\ (\Delta x)^2}{(\Delta\psi)d_6}[1 + (\frac{y_{i+1\ 1}-y_{i-1\ 1}}{2\Delta x})^2]^{1.5}$$

$$d_4 = (\Delta x)^2[-(\frac{y_{i+1\ 1}-y_{i-1\ 1}}{2\Delta x})(1+(\frac{y_{i+1\ 1}-y_{i-1\ 1}}{2\Delta x})d_7 - (1+[\frac{y_{i+1\ 1}-y_{i-1\ 1}}{2\Delta x}]^2)^{1.5} d_8]$$

$$d_5 = d_9^2[a_{11}+b_{11}d_9^{\gamma-1}]$$

$$d_6 = \sqrt{d_5}$$

$$d_7 = d_{10}(a_{11}+b_{11}\gamma d_9^{\gamma-1})d_9/d_5^2$$

$$d_8 = d_{11}/d_9\sqrt{d_5}$$

$$d_9 = (1 + \frac{\gamma M_\infty^2}{2}(C_p)_{i1})^{1/\gamma}$$

$$d_{10} = \frac{1}{2\Delta x}((d_9)_{i+1\ 1}-(d_9)_{i-1\ 1})$$

$$d_{11} = \frac{1}{\Delta\psi}(\tilde{\rho}_{i2}-(d_9)_{i1})$$

$$a_{11} = 1 + \frac{2}{(\gamma-1)M_\infty^2}, \quad b_{11} = -2/(\gamma-1)M_\infty^2 .$$

ρ and $\tilde{\rho}$ are relaxed in the same way as in Chapter III. SLOR is used to solve (4.2.1),(4.2.2). A simple algorithm that solves the equations is given below.

Step 1. Construct a computational domain and choose the grid size.

Step 2. Set:

$$y_{ij} = \begin{cases} \psi_{min} + (j-1)\Delta\psi, & \forall j>1 \\ \psi_{min} + (j-1)\Delta\psi, & j=1,\ i=i_{max} \text{ or } i_{min} \\ 0, & j=1\ i<i_{LE} \text{ or } i>i_{TE} \end{cases}$$

$$\rho_{ij} = 1, \quad \forall i,j$$

$$\tilde{\rho}_{ij} = 1 \qquad \forall_{i,j} \text{ except for } j=1,\ i_{LE} \le i \le i_{TE}$$

$$\tilde{\rho}_{ij} = \left(1+\frac{\gamma M_\infty^2}{2} C_{p_i}\right)^{1/\gamma} \qquad \text{for } j=1,\ i_{LE} \le i \le i_{TE}$$

Step 3. Central difference all the derivatives in equation (4.1.7a) everywhere except along j=1, for $i_{LE} \le i \le i_{TE}$. Along this segment,

(i) use central differencing for y_{xx}

(ii) use two point forward differencing for y_ψ

(iii) use central differencing for y_x

(iv) replace $(y_{\psi\psi})$, by

$$(Y_{\psi\psi})_{j=1} = \frac{2(y_{i2}-y_{i1})}{\Delta\psi^2} - \frac{2}{\Delta\psi}(y_\psi)_{j=1}$$

with

$$(y_\psi)_{j=1} = (b\sqrt{1+y_x^2})_{j=1}$$

(v) For speed calculations, differencing for y_x derivative is the same as used in section 3.2.

Solve (4.2.1) and (4.2.2) for y by calculating the coefficients C_k, d_m, k=1,...5, m=1,...11 at previous iteration level until the tolerance level for y is satisfied

Step 4. Calculate ρ from (3.1.8).

Step 5. Calculate $\tilde{\rho}$ from (3.1.9).

Step 6. Check the convergence for ρ, $\tilde{\rho}$. Continue iteration until convergence for ρ, $\tilde{\rho}$ and y is achieved.

4.3 FLOW EQUATIONS, NUMERICAL ALGORITHM FOR STRETCHED GRIDS

Introducing the variable Y defined by (3.4.2) and employing transformation (3.1.1, 3.1.2), the equations corresponding to (4.2.1 , 4.2.2) in the (ξ,η) system are

$$C_1[Y_{i+1j} - 2Y_{ij} + Y_{i-1j}]$$

$$+ C_2[Y_{ij+1} - 2Y_{ij} + Y_{ij-1}]$$

$$+ C_3[Y_{i+1j+1} + Y_{i-1j-1} - Y_{i-1j+1} - Y_{i+1j-1}]$$

$$+ C_4[Y_{i+1j} - Y_{i-1j}]$$

$$+ C_5[Y_{ij+1} - Y_{ij-1}] = C_6 \quad , \tag{4.3.1}$$

and

$$B_1[Y_{i+1\,1} - 2Y_{i1} + Y_{i-1\,1}]$$

$$+ 2B_2\beta^2[Y_{i\,2} - Y_{i\,1}]$$

$$+ B_3\frac{(\Delta\xi)}{2}[Y_{i+1\,1} - Y_{i-1\,2}] = B_4 + B_5 \tag{4.3.2}$$

where

$$C_1 = A_1$$

$$C_2 = \frac{(\Delta\xi)^2 A_2}{(\Delta\eta)^2}$$

$$C_3 = \frac{(\Delta\xi)^2 A_3}{4\Delta\xi\Delta\eta}$$

$$C_4 = \frac{(\Delta\xi)^2 A_4}{2\Delta\xi}$$

$$C_5 = \frac{(\Delta\xi)^2 A_5}{2\Delta\eta}$$

$$C_6 = (\Delta\xi)^2 A_6 \; \psi_\eta^2 x_\xi^2$$

$$B_1 = \psi_\eta^2 (1-B_6)/B_7$$

$$B_2 = x_\xi^2 [1+B_6]$$

$$B_3 = -\frac{x_{\xi\xi}}{x_\xi} B_1$$

$$B_4 = [2\frac{(\Delta\xi)^2}{(\Delta\eta)} - (\Delta\xi)^2 B_8] B_9$$

$$B_5 = (\Delta\xi)^2 x_\xi^2 \psi_\eta^2 [-\frac{\sqrt{B_6}}{x_\xi}(1+B_6)B_{10} - \frac{1}{\psi_\eta}(1+B_6)^{3/2} B_{11}]$$

$$B_6 = \frac{1}{x_\xi}[\frac{Y_{i+1\ i} - Y_{i-1}}{2\Delta\xi}]$$

$$B_7 = B_{12}^2 [a_1^* + b^* B_{12}^{\gamma-1}]$$

$$B_8 = -B_2 \frac{\psi_{\eta\eta}}{\psi_\eta}$$

$$B_9 = \frac{\psi_\eta \sqrt{1+B_6}}{\sqrt{B_7}}$$

$$B_{10} = B_{13}(a_1^* + b^* \gamma B_{12}^{\gamma-1}) B_{12}/B_7^2$$

$$B_{11} = \frac{1}{B_{12}\sqrt{B_7}} (\frac{\tilde{\rho}_{i2} - (B_{12})_{i1}}{\Delta\eta})$$

$$B_{12} = \left(1 + \frac{\gamma M_\infty^2}{2} C_{p_{i1}}\right)^{1/\gamma}$$

$$B_{13} = \frac{1}{2\Delta x}\left[(B_{12})_{i+1\ 1} - (B_{12})_{i-1\ 1}\right]$$

where A_i's i=1,...6, are given in (3.4). The equation (4.3.1) can easily be written in the matrix form as before.

The numerical algorithm for (4.3.1-4.3.2) is the same as given in section 4.2.

4.4 RESULTS AND DISCUSSION

Calculations for various subcritical and supercritical flow configurations have been carried out on both uniform and stretched grids using the algorithm described in Section 4.2. Input pressure distributions used in the calculations were taken to be those which were numerically computed using the full potential formulation of the direct problem as described in Chapter III. Results of the computations are shown in figures (13-20).

Figures (13-14) show comparison of the exact and numerically obtained coordinates for the NACA 0012 airfoil at $M_\infty = 0.63$. The loss of accuracy near the leading edge in Fig.(13) is the result of the input pressure distribution which was not very accurate near the leading edge. However, these inaccuracies have been eliminated by using more accurate input data computed on a fine grid (Fig.14).

The exact and numerically obtained coordinates for the NACA 0012 airfoil at $M_\infty = 0.7$ are illustrated in Fig (15). The numerical results are in good agreement with the exact values.

Figures (16 and 17) compare computed coordinates for a 6% circular arc airfoil at $M_\infty = 0.817$ with the exact airfoil shape. Again the results for this subcritical flow are excellent.

Figures (18 and 19) show the results for a supercritical flow at $M_\infty = 0.8$ on the NACA 0012 airfoil. Our results show some inaccuracies near the leading edge when computed on a coarse grid. However, these inaccuracies have been greatly reduced by carrying out the calculation on a finer grid (Fig. 20). We point out that in our calculations, numerically computed data was used. During the investigation, we found that even a slight change in the input data affects the shape of the body. If the best available input data is used, we expect that the discrepancies in the airfoil coordinates mentioned above can be essentially eliminated.

In the programmes, the relaxation parameters w_1, w_2 and constants A, B, D appearing in the stretching functions (3.3.1 and 3.3.2) are taken to be the same as in Chapter III. Conventional design methods require the solution of a sequence of direct problems, with

the airfoil converging to the required shape. Various optimization routines have been developed to minimize the number of direct problems to be solved. In our formulation we only have to solve one problem which has mixed Dirichlet and Neumann boundary conditions. The solution of this inverse problem provides the airfoil shape, given by $y(x_i,0)$, i.e., y_{il} for $i_{LE} \leq i \leq i_{TE}$.

The computational information for the numerical design of the NACA 0012 and 6% circular arc airfoils, giving the number of iterations and CPU times for various Mach numbers and grid sizes, is summarized in Tables 4 and 5.

CHAPTER V

LIFTING PROBLEMS

In Chapters III and IV we studied inviscid compressible flow past symmetric airfoils at zero incidence. In the present chapter we will study flow past symmetric airfoils at incidence. Incompressible flow around airfoils is also considered because the present method has not previously been used in this application. The analysis and numerical procedure is then extended to compressible flows. The flow equations and numerical results are presented here.

5.1 FLOW EQUATIONS AND BOUNDARY CONDITIONS

The non-dimensional equations describing the irrotational flow of an inviscid incompressible fluid in the (x,ψ)-plane are [24],

$$y_\psi^2 y_{xx} - 2y_x y_\psi y_{x\psi} + (1+y_x^2) y_{\psi\psi} = 0 \quad \text{(vorticity equation)} \tag{5.1.1}$$

$$y_\psi^2 v^2 = 1 + y_x^2 \quad \text{(equivalent form of continuity equation)} \tag{5.1.2}$$

$$1 + y_x^2 + 2py_\psi^2 = C_o y_\psi^2 \quad \text{(Bernoulli's equation)} \tag{5.1.3}$$

where

$$v^2 = u^2 + v^2 \ , \quad C_o = \text{constant of integration},$$

p is the pressure and u,v are the components of the velocity.

Recall from Chapter III that the non-dimensional equations governing the irrotational flow of an inviscid, isentropic, compressible fluid in the (x,ψ)-plane are

$$y_\psi^2 y_{xx} - 2y_x y_\psi y_{x\psi} + (1+y_x^2) y_{\psi\psi} = \frac{y_x y_\psi^2 \rho_x}{\rho} - \frac{y_\psi (1+y_x^2)\rho_\psi}{\rho} \tag{5.1.4}$$

$$\frac{2\rho^{\gamma-1}}{(\gamma-1)M_\infty^2} + \frac{1+y_x^2}{\rho^2 y_\psi^2} = 1 + \frac{2}{(\gamma-1)M_\infty^2} . \tag{5.1.5}$$

The appropriate boundary conditions for either incompressible or compressible flow in the physical plane are

$$\frac{v}{u} = f_\pm'(x) \qquad \text{for } x_{LE} \le x \le x_{TE},\ y = f(x)$$
(tangency condition) (5.1.6)

$$V = 0 \qquad \text{at TE (Kutta condition)} \tag{5.1.7}$$

$$y\cos\alpha - x\sin\alpha + \Gamma^* \ln(x^2+my^2) - \psi = 0$$
(along outer boundaries) (5.1.8)

where α is the angle of attack, Γ^* is a constant proportional to the circulation Γ, $\Gamma^* = \frac{1}{2}\Gamma$ and where

$$m = \begin{cases} 1 , & \text{for incompressible fluid} \\ 1 - M_\infty^2 , & \text{for compressible fluid,} \end{cases}$$

and

(±) indicate upper and lower surface respectively. Condition (5.1.6) states that there is no flow through the airfoil. The Kutta condition (5.1.7) asserts that the flow should leave smoothly from the trailing edge.

Equation (5.1.8) is the condition that the stream-function far away from the body is due to a uniform flow and a vortex [40]. The Kutta condition, employing Bernoullis' equation, is equivalent to the requirement that pressure and speed are continuous at the trailing edge, i.e.,

$$(V_+^2)_{TE} = (V_-^2)_{TE} \quad . \tag{5.1.9}$$

In the (x, ψ)-plane, considering the airfoil as a segment of the streamline $\psi=0$, equation (5.1.6) is replaced by

$$y = f_\pm(x) \quad \text{for } x_{LE} \leq x \leq x_{TE},\ \psi=0 \quad . \tag{5.1.10}$$

Therefore, the well-posed boundary value problems for the incompressible and compressible case, respectively, are

Incompressible

$$y_\psi^2 y_{xx} + (1+y_x^2) y_{\psi\psi} - 2y_x y_\psi y_{x\psi} = 0$$

subject to

$$y = f_\pm(x) \quad \text{for } x_{LE} \leq x < x_{TE},\ \psi=0$$

$$\left[\left(\frac{1+y_x^2}{y_\psi^2} \right)_- \right]_{TE} = \left[\left(\frac{1+y_x^2}{y_\psi^2} \right)_+ \right]_{TE}$$

$$\psi = y\cos\alpha - x\sin\alpha + \Gamma^* \ell n(x^2+y^2) \text{ at } \infty \quad .$$

2. Compressible

$$y_\psi^2 y_{xx} + (1+y_x^2)y_{\psi\psi} - 2y_x y_\psi y_{x\psi} = \frac{y_x y_\psi^2 \rho_x}{\rho} - \frac{y_\psi(1+y_x^2)\rho_\psi}{\rho}$$

$$\frac{2\rho^{\gamma-1}}{(\gamma-1)M_\infty^2} + \frac{1+y_x^2}{\rho^2 y_\psi^2} = 1 + \frac{2}{(\gamma-1)M_\infty^2}$$

$$y = f_\pm(x) \qquad \text{for } x_{LE} \leq x \leq x_{TE} \ , \ \psi=0$$

$$\left[\left(\frac{1+y_x^2}{\rho^2 y_\psi^2}\right)_- \right]_{TE} = \left[\left(\frac{1+y_x^2}{\rho^2 y_\psi^2}\right)_+ \right]_{TE}$$

$$\psi = y\cos\alpha - x\sin\alpha + \Gamma^* \ell n(x^2 + (1-M_\infty^2)y^2) \text{ at } \infty \quad .$$

5.2 METHOD OF SOLUTION

For the compressible case the artificial density $\tilde{\rho}$ is introduced in exactly the same way as in Chapter III. In order to solve these boundary value problems, following Jones [31], we divide the computational domain into four regions as shown in Figure [21]. We then sweep each region in succession by employing line relaxation. To apply line relaxation, we employ old values of y and $\tilde{\rho}$ at mesh points to represent first derivatives

$$y_x \doteq \frac{y_{i+1j} - y_{i-1j}}{2\Delta x}$$

$$y_\psi \doteq \frac{y_{ij+1} - y_{ij-1}}{2\Delta\psi}$$

$$\tilde{\rho}_x \doteq \frac{\tilde{\rho}_{i+1j} - \tilde{\rho}_{i-1j}}{2\Delta x}$$

$$\tilde{\rho}_\psi \doteq \frac{\tilde{\rho}_{ij+1} - \tilde{\rho}_{ij-1}}{2\Delta\psi} .$$

For derivatives y_{xx}, $y_{\psi\psi}$, we employ respectively,

$$y_{xx} \doteq \frac{y_{i+ij} - 2y^+_{ij} + y_{i-1j}}{\Delta x^2}$$

$$y_{\psi\psi} \doteq \frac{y^+_{ij+1} - 2y^+_{ij} + y^+_{ij-1}}{\Delta\psi 2} .$$

Here superscript (+) indicates a new value of the unknown y.

In region I, when relaxation is applied at the point $(I_1-1,0)$, we require the value of $\tilde{\rho}$ at $(I_1,0)$ and this is set to be equal to $\tilde{\rho}$ at $(I_1-1,0)$. Likewise the value of density $\tilde{\rho}$, in region IV, at $(I_2,0)$ is set equal to the value of $\tilde{\rho}$ at $(I_2+1,0)$.

In regions II and III, on the airfoil, we employ the following expressions for y_ψ, y_x:

$$y_\psi \doteq \frac{y_{iS^+} - f_+(x)\,|_i}{\Delta\psi} \qquad \text{in region II}$$

$$y_\psi \doteq \frac{y_{iS^-} - f_-(x)\,|_i}{\Delta\psi} \qquad \text{in region III}$$

$$y_x = f'_{\pm}(x) \qquad (5.2.1)$$

where (±) indicates the value at the upper and lower surfaces respectively and

y_{iS^+} : value of y at i on the streamline S^+ which is above the streamline $\psi=0$

y_{iS^-} : value of y at i on the streamline S^- which is below the streamline $\psi=0$.

To calculate speed at grid point (i, j), y_x is computed from

$$y_x \doteq \frac{y_{i+1j} - y_{i-1j}}{2\Delta x} \quad \text{(in subsonic region)}$$

$$y_x \doteq \frac{y_{ij} - y_{i-2j}}{2\Delta x} \quad \text{(in supersonic region)}$$

except along $\psi=0$, $x_{LE} \leq x \leq x_{TE}$, where (5.2.1) is employed.

In each region the differenced equations can easily be written in the matrix form

$$M\bar{Y} = \bar{B} \qquad (5.2.2)$$

exactly the same way as in Chapter III.

The circulation Γ around the airfoil is determined such that at the trailing edge, the speeds V_{up} at the upper surface and $V_{\ell o}$ at the lower surface are equal. Following [41], the iterative procedure

$$\Gamma^{(n+1)} = \Gamma^{(n)} + \beta_o(V_{up} - V_{\ell o}) \qquad (5.2.3)$$

is employed. In equation (5.2.3), β_0 is the relaxation parameter and for our purpose we take

$$.17<\beta_o<.31 \ . \tag{5.2.4}$$

The procedure employed to determine the range β_o is described in the flow diagram (1).

The iterative algorithm for the incompressible and the compressible case are represented by flow diagrams (2 and 3), respectively.

The pressure coefficient C_p and lift coefficient C_L are computed from

$$\left.\begin{aligned} C_p &= 1 - \frac{(1+y_x^2)}{y_\psi^2} \\ C_L &= 2\Gamma \end{aligned}\right\} \quad \text{incompressible} \tag{5.2.5}$$

$$\left.\begin{aligned} C_p &= \frac{2}{\gamma M_\infty^2}(\tilde{\rho}^{\gamma}-1) \\ C_L &= 2\int_0^1 (C_{p\ell}-C_{pu})dx \end{aligned}\right\} \quad \text{compressible} \tag{5.2.6}$$

5.3 RESULTS AND DISCUSSION

The algorithm described in diagrams (2 and 3) has been used for the computation of incompressible and compressible flows over NACA 0012 and 6% circular arc airfoils at different angles of incidence.

Figures(22-24)show pressure distributions for incompressible flow on a NACA 0012 airfoil for angles of attack 4°, 6° and 8°, respectively. Comparison is made with the numerical results obtained by Carey and Kim [42]. In the case of a 4° angle of attack, our result agrees very well with Carey's results. For angles of attack 6° and 8° there appear to be some discrepancies in the pressure distributions although the accuracy of Carey's results is not known. Lift coefficient C_L is plotted against angle of attack α in Fig.(25)and shows excellent agreement with the results of [42] and Abbot and Von Doenhoff [43].

For compressible flow, the computed pressure distributions on the NACA 0012 and 6% circular arc airfoils are illustrated in Figures(26)to (30). Figures (26) and (27) show comparison of pressure distributions for the 6% circular arc airfoil at $M_\infty = 0.706$ for α=.5° and 1°. Comparison is made with the experimental results of Earl [35], and our results are in excellent agreement.

The pressure distribution on the streamline ψ=0 for the NACA 0012 airfoil at $M_\infty = 0.8$ and α=10° is illustrated in Fig.(28)in which comparison is made with the results of Hafez et al. [41]. Our results show good agreement with theirs.

Figure (29) shows the pressure distribution on a

NACA 0012 airfoil at $M_\infty = 0.75$ and $\alpha = 1.0°$. This figure indicates that there are some discrepances in our results. These discrepancies may be due to the type of differencing used, i.e.; we used a non-conservative form of the governing equation while conservative differencing was used in reference [44]. Such discrepancies in the pressure distribution are also reported in [45] (see Fig. 29). Figure (30) shows the pressure distribution for a NACA 0012 airfoil at $M_\infty = 0.75$ and $\alpha=2°$. Comparison has been made with reference [45].

Convergence history for the circulation, which is updated at each global y iteration are presented in Figures (31) and (32).

Our results indicate that the present formulation for lifting cases produces very good results over a wide range of Mach numbers and angles of attack. It also provides Dirichlet boundary conditions over the airfoil and in the far field. The Kutta condition is easily satisfied and there is no need to do grid generation since it is automatically taken care of by the stream function coordinate formulation. Tables 6 and 7 summarize the computational information for the NACA 0012 and 6% circular arc airfoils, giving the number of iterations, grid sizes, Mach numbers and angles of attack.

CHAPTER VI.

CONCLUSION

In this dissertation a new formulation is proposed for solving the steady 2-D inviscid transonic flow past airfoils, considering both the analysis and design modes.

Historically, researchers have relied heavily on the irrotational character of such flows and this has lead to numerous studies involving the velocity potential formulation. In the potential formulation, the unknowns Φ (potential) and ρ (density) are obtained as solutions of the partial differential equation for conservation of mass and an algebraic equation for the density, the well-known Bernoulli's equation. The first successful finite difference solution of the small-disturbance potential equation for supercritical transonic flow seems to be due to Murman and Cole [11], using a type-dependent differencing scheme. The small-disturbance approximation provides two main advantages. First, the density can be expressed explicitly as a function of the derivative of the velocity potential and hence a single nonlinear equation for Φ can be solved. Secondly, the boundary condition on the airfoil surface is transferred to the airfoil chordline which, for symmetric airfoils at small incidence, means that the physical domain is rectangular

(no curved boundaries) and is convenient for finite difference calculations.

Extensions to the full-potential equation were made possible with the advent of grid generation technology. Grid generation allowed CFD researchers to numerically map the physical solution domain, which has at least part of its boundary as the curved airfoil surface, into a rectangular computational domain. The flow equations can then be transformed and solved by the finite difference method on this rectangular domain. Jameson [26,27,29] developed some of the early methods for handling the full-potential equation for transonic subcritical and supercritical flows. In order to account for the correct differencing in the subsonic and supersonic regions of a supercritical flow, Jameson introduced the concepts of rotated differences [26] and artificial viscosity [29]. These schemes, and various modifications and extensions, are still in use today, indicating the importance of Jameson's initial contributions. One modification of the artificial viscosity method which has gained some confidence over recent years is the artificial density method developed by Hafez and others [19,28,30]. This method is based on the same fundamental ideas as Jameson's artificial viscosity method, using a switching parameter to provide the necessary amount of upwinding for the

finite difference approximation in the supersonic region. To date no researcher has provided a better method to account for the change in the mathematical character of the flow equation as one moves from the subsonic (elliptic) to the supersonic (hyperbolic) region. In this work we have used both the artificial density method and the type-dependent differencing method.

One significant feature of the potential formulation is that it can be extended rather easily to 3-D flows [14]. However, the most serious limitation of the potential formulation is its inability to account for entropy changes which occur due to the shock wave which forms over the airfoil. In reality, transonic flows are rotational and hence a velocity potential does not exist. In terms of the level of sophistication of the mathematical model, one wants to move from the equations for potential flow to the Euler equations which account for rotational effects and entropy changes. This motivated researchers to consider a streamfunction formulation as an alternative to the potential formulation [19]. The streamfunction formulation can easily be extended to allow for vorticity. As with the potential formulation, grid generation is an important first step in the numerical solution of the equation for the streamfunction. In general, the boundary conditions in the streamfunction formulation are simpler

than in the potential formulation, being Dirichlet rather than Neumann on the airfoil surface. However, extensions to 3-D are cumbersome because of the need to define a pair of streamfunctions and most researchers have, therefore, abandoned this approach in favor of a primitive variable formulation of the Euler equations.

One chapter in this dissertation deals with the inverse or design problem in which the surface pressure distribution is prescribed and the corresponding airfoil surface is an unknown to be determined. This problem is of particular importance to the designer since his or her job is to construct an airfoil with a given set of performance conditions. The classical approach to airfoil design has been to make an educated guess (based largely on experience) as to the required airfoil shape. A direct calculation based on this assumed shape is then carried out (analysis mode) and the calculated pressure distribution is compared to the desired one. If these do not agree then the airfoil shape is adjusted according to some pre-determined set of rules. The pressure distribution is recalculated for this new airfoil and compared to the prescribed one, etc. This iterative process is continued until the calculated and prescribed pressures match. Considerable efforts have been made to optimize this iterative procedure so that a minimum number of airfoil shapes need to be analyzed.

Virtually all finite difference calculations for realistic airfoil geometries rely heavily on some form of numerical grid generation, whether it be via conformal mapping, algebraic, elliptic or hyperbolic grid generation. Thompson et al [21] have provided an extensive survey of this field up to and including 1982. The high level of current research activity in grid generation is clearly an indication of the importance of this technology to the computational fluid dynamicist, and several very successful grid generation codes are commercially available. Although grid generation is an integral part of the current state-of-the-art in CFD it has its own limitations and drawbacks. Certainly, iterative adjustment of the grid is necessary to accurately predict the flow in regions of high gradients and use of adaptive grids is becoming indispensible in this regard. Furthermore considerable CPU time is required to solve the grid generation equations and, for fine grid calculations, large storage is needed to save the grid for the solution of the actual flow equations. Also, as is common when one uses commercial packages, user experience is an important factor in successfully achieving the correct physical solution.

In this dissertation we have attempted to address some of the limitations and difficulties discussed above. In short, a formulation is proposed which, (i) eliminates the numerical grid generation process, (ii) can be extended

to rotational flows and 3-D flows, (iii) provides a Dirichlet boundary value problem for the analysis mode and, (iv) provides a mixed boundary value problem for the design mode which can be solved numerically to determine the desired airfoil shape as part of the overall finite difference solution. All of these features are achieved as a result of a formulation of the flow equations in von Mises coordinates (x, ψ) in which the y and ρ are treated as the unknowns. Two approaches are employed to solve the governing equations subject to appropriate boundary conditions.

In the first approach artificial density is introduced in the flow equations following Hafez and Lovell [19]. The flow equation is discretized using centered differences for all the derivatives everywhere in the computational domain. In density calculations, type-dependent differencing is used for y_x to account for upwinding in the supersonic region. Numerical calculations are made using successive line overrelaxation method for NACA 0012 and 6% circular arc airfoils at different Mach numbers and angles of attack. Results obtained are in good agreement with experimental and other numerical results. In this approach, we fail to achieve convergence for y on a fine grid, for example, on a grid having more than 39 points over airfoil, for the supercritical case. This is, perhaps, due to the freezing of the terms containing density derivatives and the use of artificial density in the flow equation which inherently

introduces a numerical error in the solution as indicated by Essers [32]. Other researchers have also indicated the difficulties in achieving convergence on fine grids, for example, see Wigton [34].

After some numerical experimentation, it was found that the choice of switching parameter μ in the artificial density method strongly affects the convergence. A survey of the literature indicates researchers have used different forms of the switching parameters to make their schemes converge, for example, Holst [44,45] explicitly mentions that his scheme fails to converge for a different choice of μ. The proper choice of μ comes mainly from experience or numerical experimentation. We believe that the convergence on a fine grid may be achieved in the von Mises formulation if one can determine an appropriate form for μ.

From the above, we conclude that as the number of gnid points are increased, it is very hard to achieve convergence. To accomplish it, researchers modify μ or use some strategy to damp out drastic change in the flow variables [34]. To eliminate these aforementioned difficulties, we use a second approach in which an alternate form of the irrotationality condition is obtained independent of density derivative terms. This is done by eliminating ρ_x and ρ_ψ from the irrotationality condition using the momentum equations. The resulting equation is solved

using type-dependent differencing and to avoid drastic change in density in the supersonic region a strategy similar to Wigton [34] is employed. In this strategy, after updating density at the grid point (i,j), we ensure that it neither drops by more than $\Delta x\%$ of $\min(\rho_{ij}^{(n)}, \rho_{i-ij}^{(n+1)}, \rho_{i+1,j}^{(n)})$ nor exceeds by more than $\Delta x\%$ of $\max(\rho_{ij}^{(n)}, \rho_{i-1j}^{(n+1)}, \rho_{i+1j}^{(n)})$. In this way, we are able to achieve convergence on fine grids.

The computed results are in good agreement with experimental or numerical results obtained by other researchers.

The main advantages of this new formulation have already been discussed. An additional advantage is that the variable y is continuously differentiable through the entire flow region. To solve lifting problems in the velocity potential formulation a jump condition on ϕ must be imposed along the rear stagnation streamline to account for the circulation. No such condition is needed for y. Finally, we point out that the coding for the von Mises formulation is extremely simple.

The method is being extended to flow over non-symmetric airfoils at incidence, axisymmetric flows, flow through cascades, flow through porous media and three dimensional incompressible flows over wing-bodies. The method can

easily be extended to study subcritical and supercritical rotational inviscid flow past bodies in two and three dimensions. Lastly, we point out that one may encounter in the von Mises formulation a non-uniqueness problem in solving the inviscid Euler equations since it is not clear to researchers how a purely inviscid solution is uniquely determined in other formulations.

FIGURES

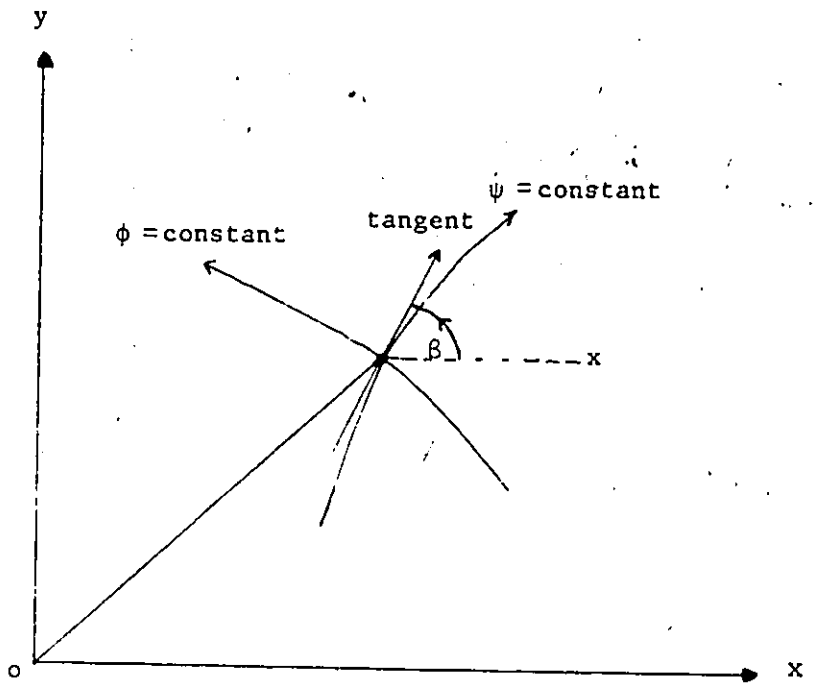

Fig. 1. (ϕ, ψ) Coordinate System.

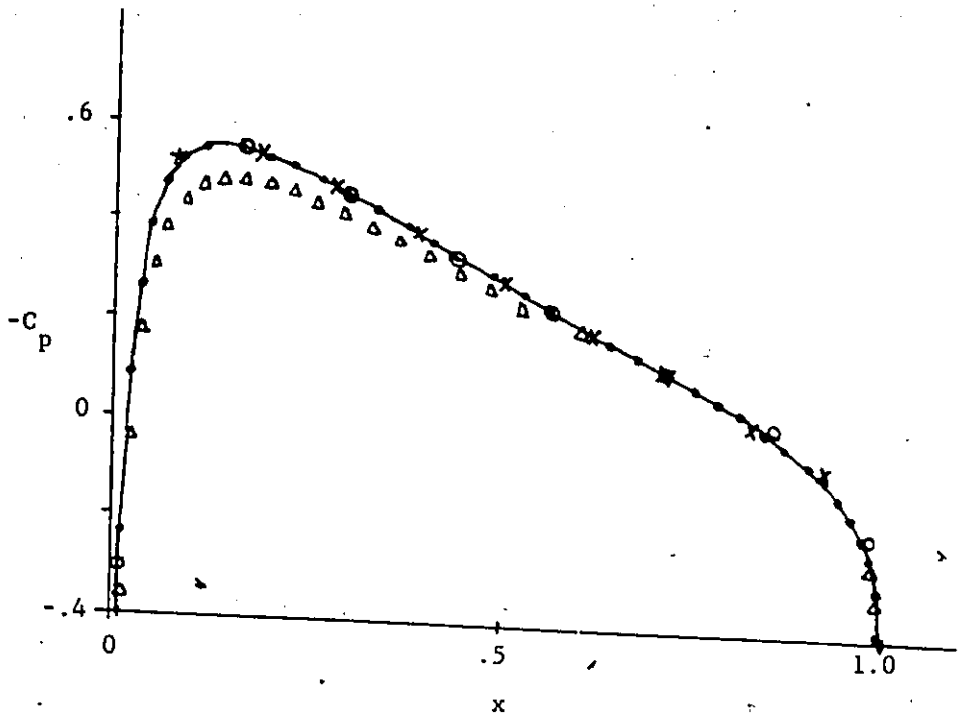

Fig. 2. Surface pressure distribution, NACA 0012
M_∞=0.63

Δ Panel Method (c.f.[33])

. . Sinclair [33]

— Garabedian-Korn [14]

o Present(un-stretched grid)

x Present (stretched grid)

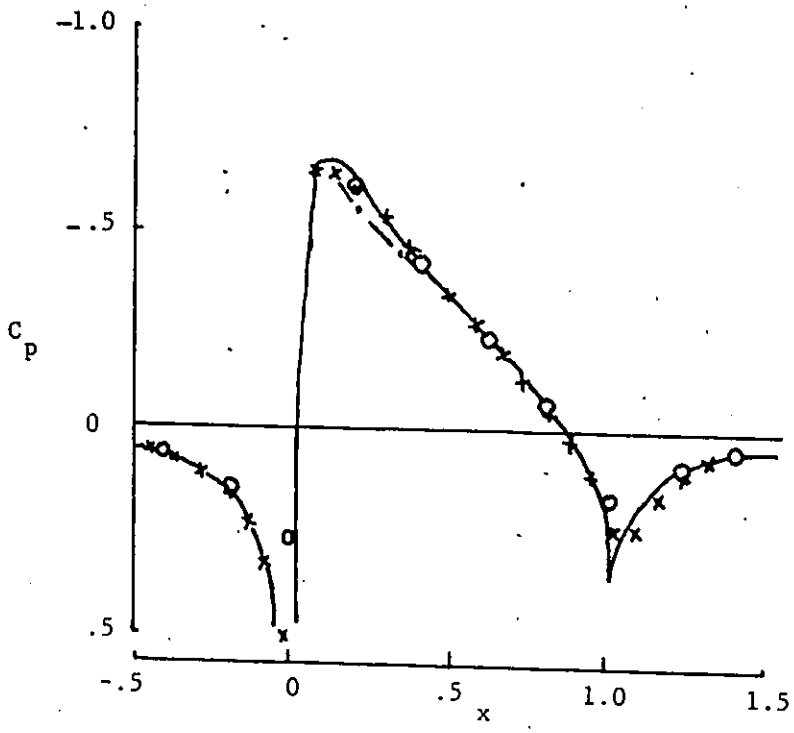

Fig. 3. Surface pressure distribution, NACA 0012, M_∞=0.7

—.— Irrotational [c.f.(19)]

—— Hafez & Lovell [19]

o Present (un-stretched grid)

-x- Present (stretched grid)

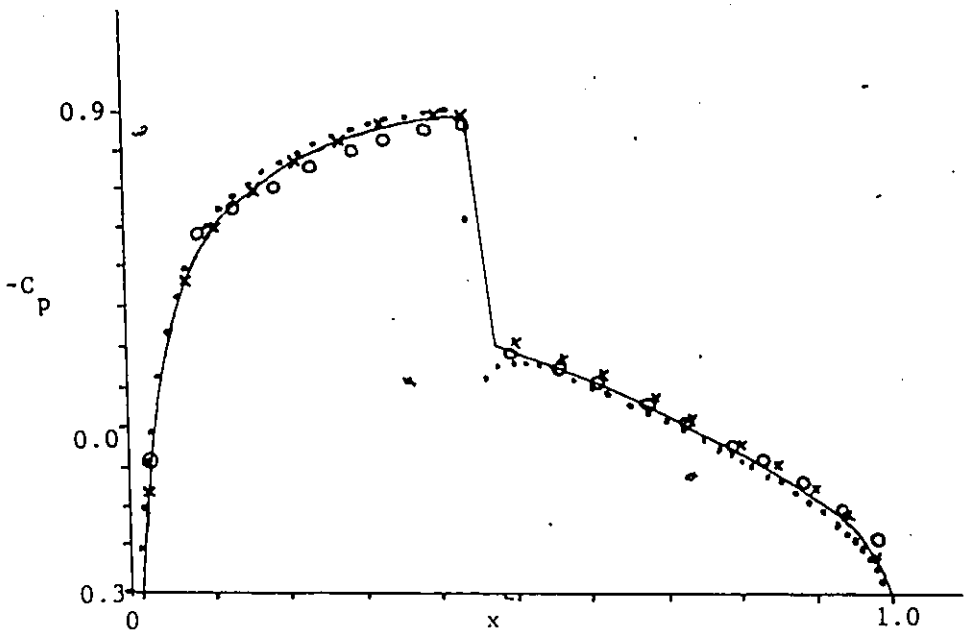

Fig. 4. Surface pressure distribution NACA 0012 M_∞=0.8.

... Sinclair [33]

—— Garabedian-Korn [14]

o Present (un-stretched grid)

-x- Present (stretched grid)

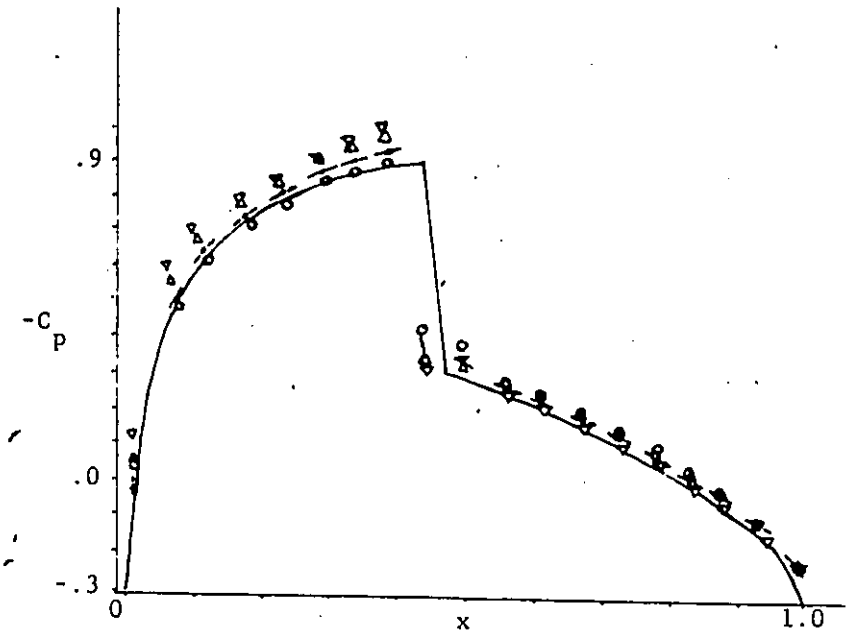

Fig. 5. Convergence of the solution for NACA 0012 at M_∞=0.8

——— Garabedian-Korn [14]

▽ C = 1.6

△ C = 2.1

-·- C = 2.6

o C = 2.9

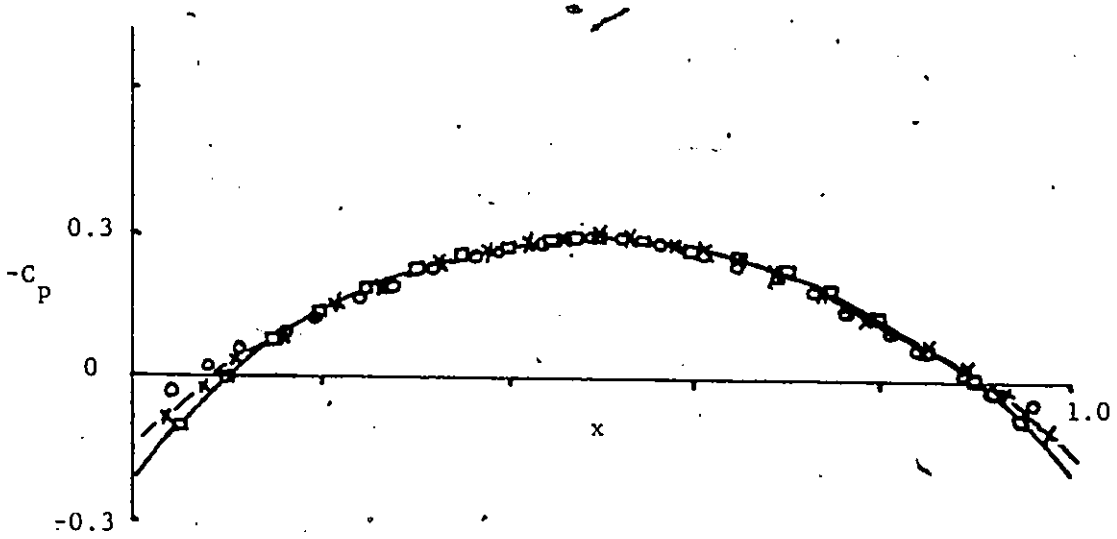

Fig. 6. Surface pressure distribution, 6% circular arc airfoil, M_∞=0.817

—□— Earl [35] - experimental

o Present (un-stretched grid)

—x— Present (stretched grid)

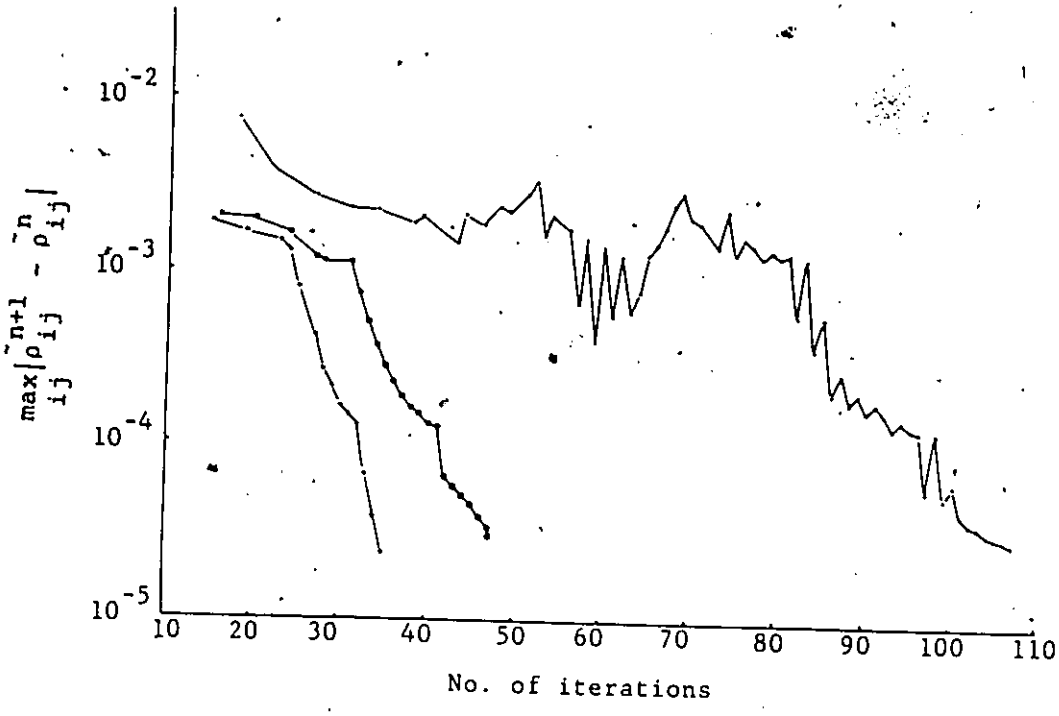

Fig. 7. Convergence histories for $\tilde{\rho}$; NACA 0012

\+ : M_∞ = 0.63

0 : M_∞ = 0.7

· M_∞ = 0.8

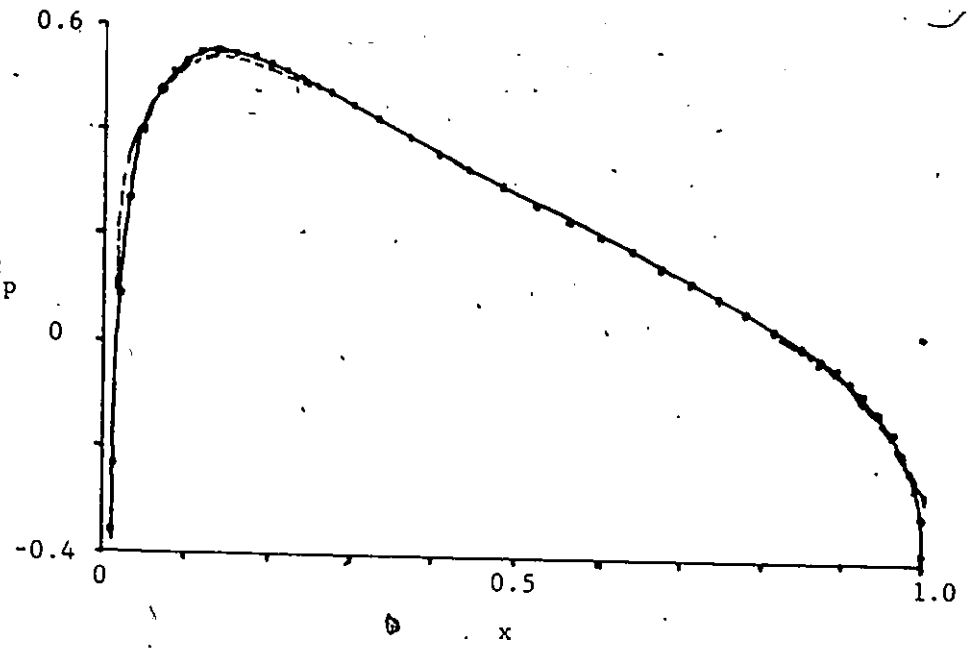

Fig. 8. Surface pressure distribution, NACA 0012, M_∞=0.63

. . . Sinclair [33]

——— Garabedian [14]

- - - Present (stretched grid, 70 surface points)

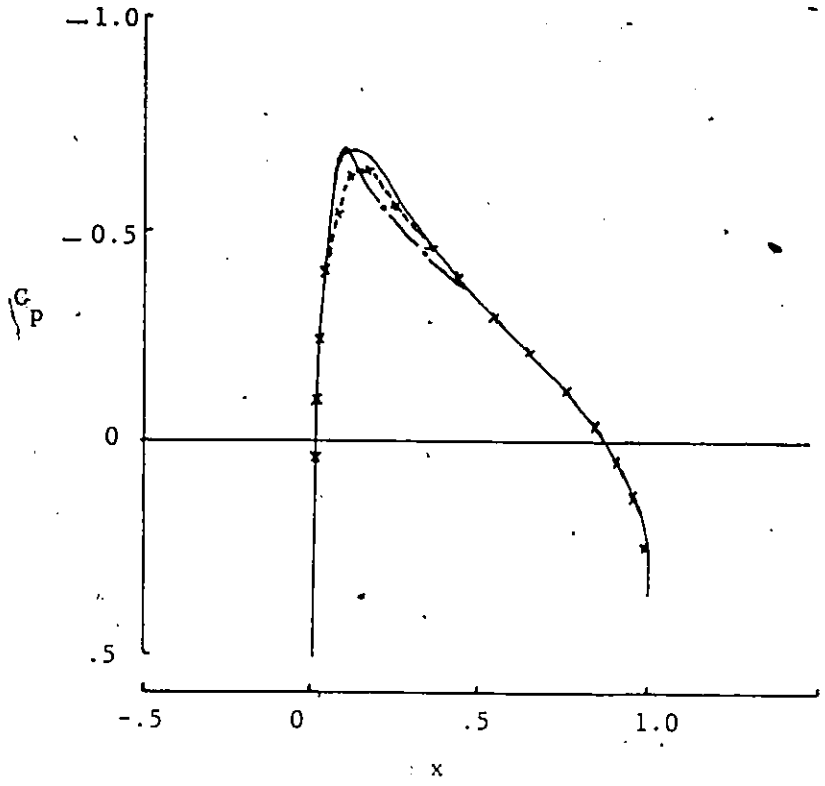

Fig. 9. Surface pressure distribution, NACA 0012, M_∞=0.7

—·— Irrotational (c.f. [19])

- - - Exact B.C. (c.f. [19])

—— Hafez and Lovell [19]

x Present (stretched grid, 70 surface points)

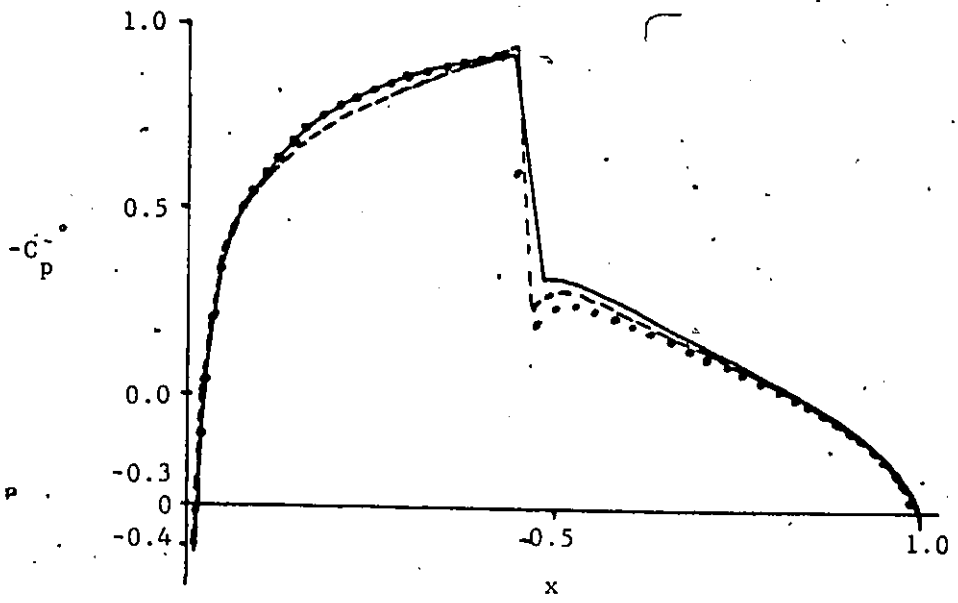

Fig. 10. Surface pressure distribution, NACA 0012, M_∞=0.8

... Sinclair [33]

—— Garabedian-Korn [14]

--- Present (stretched grid, 60 surface points)

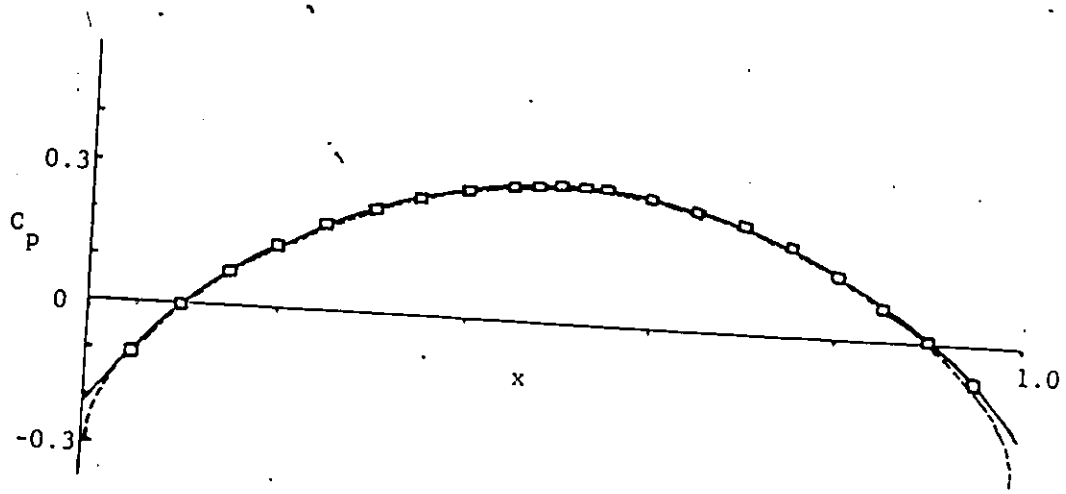

Fig. 11. Surface pressure distribution, 6% circular arc airfoil, M_∞=0.817.

—□— Earl [35], experimental

--- Present (stretched grid, 70 surface points)

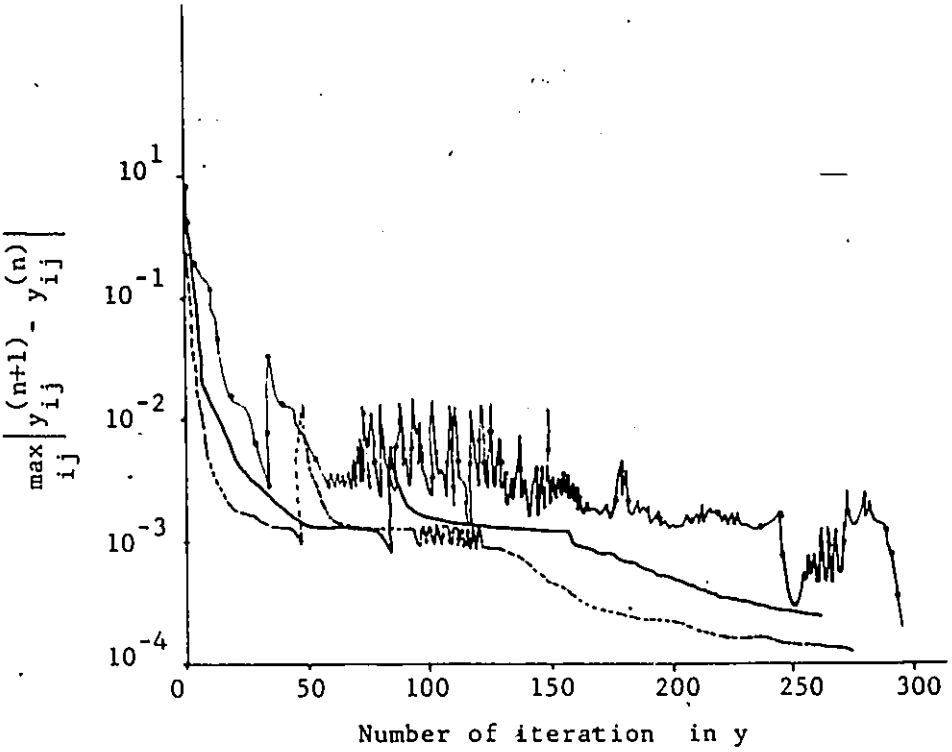

Fig. 12. Convergence history for y.

--- 6% circular arc airfoil, M_∞=0.817

—— NACA 0012, M_∞=0.63

—•— NACA 0012, M_∞= 0.8

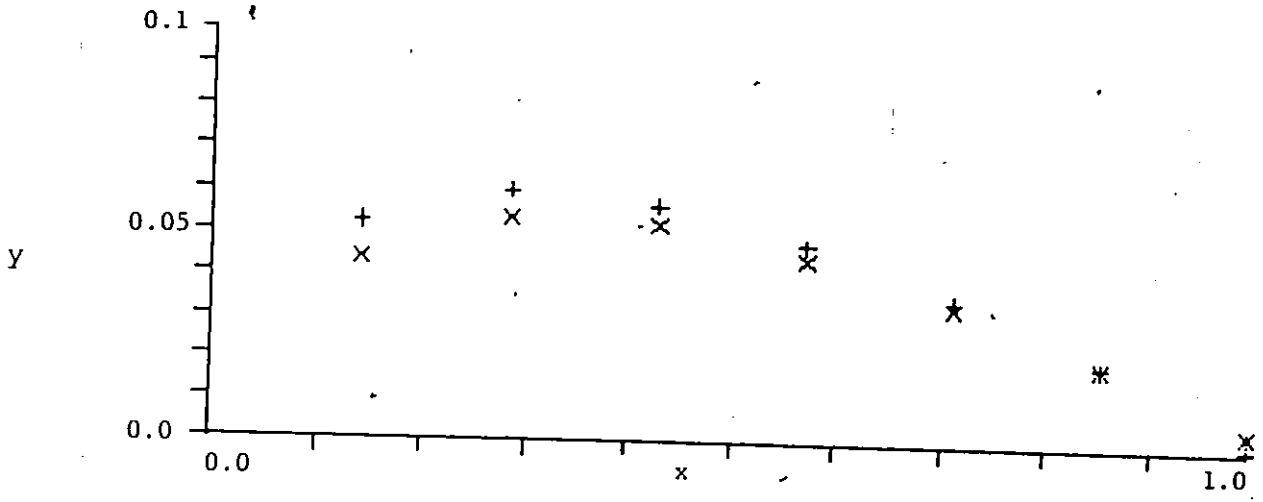

Fig. 13. A comparison between the body geometry calculated by the present method and exact body for NACA 0012 airfoil at M_∞=0.63 in un-stretched coordinates.

\+ - exact

x - computed

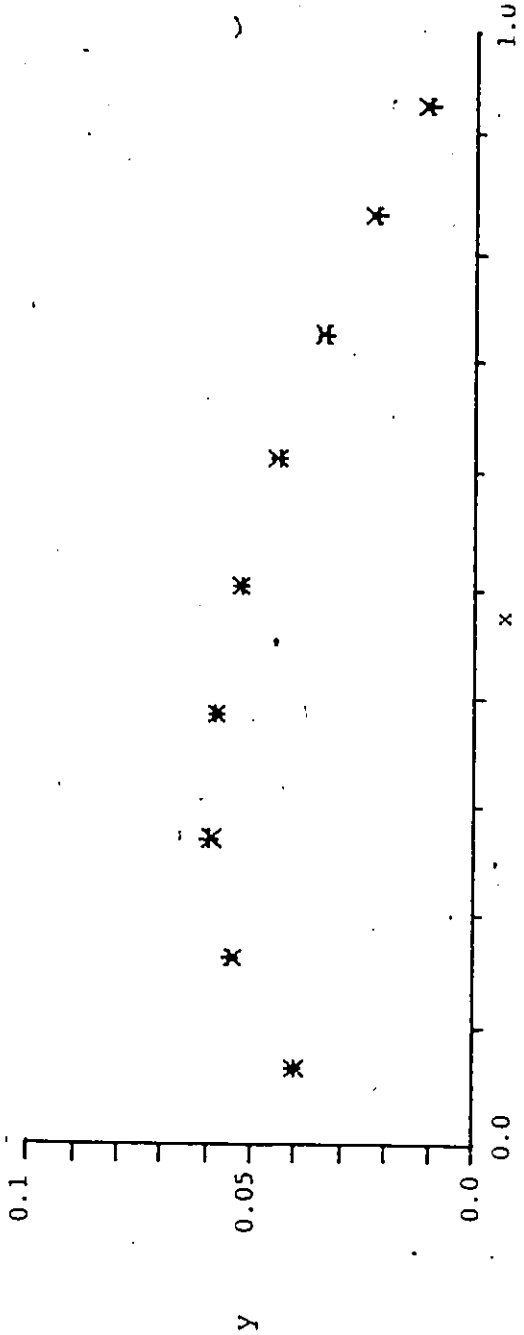

Fig. 14. A comparison between the body geometry calculated by the present method and exact body for NACA 0012 airfoil at M_∞=0.63 in stretched coordinates.

\+ - exact

x - computed

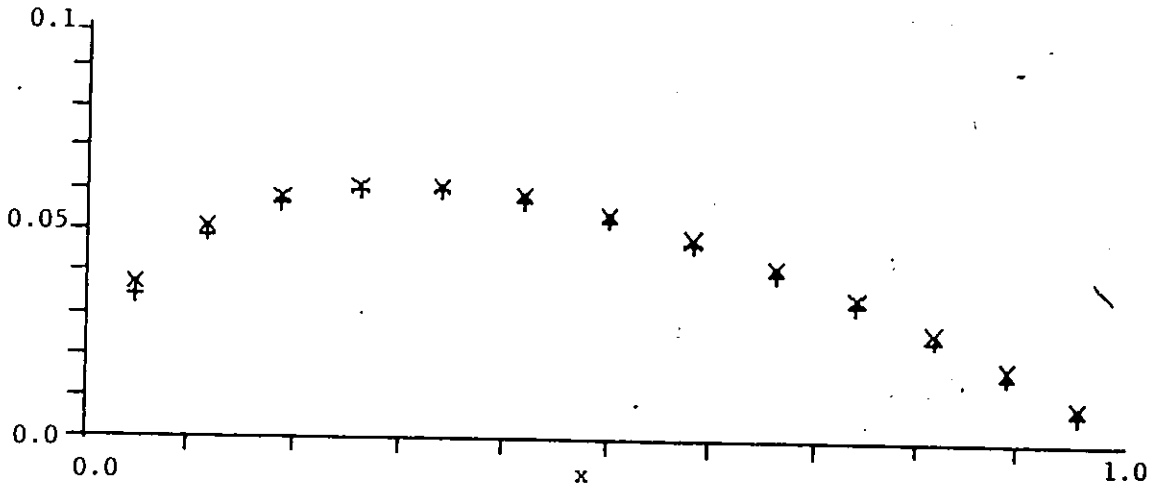

Fig. 15. A comparison between the body geometry calculated by the present method and exact body for NACA 0012 airfoil at M_∞=0.7 in stretched coordinates.

+ - exact

x - computed

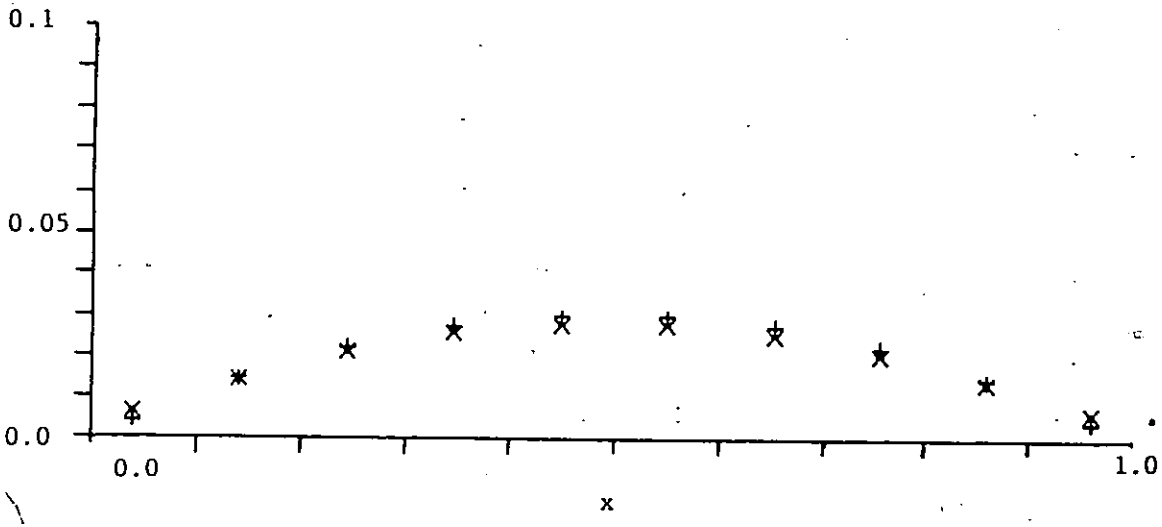

Fig. 16. A comparison between the body geometry calculated by the present method and exact body for a 6% circular arc airfoil at M_∞=0.817 in un-stretched coordinates.

+ : exact

x : computed

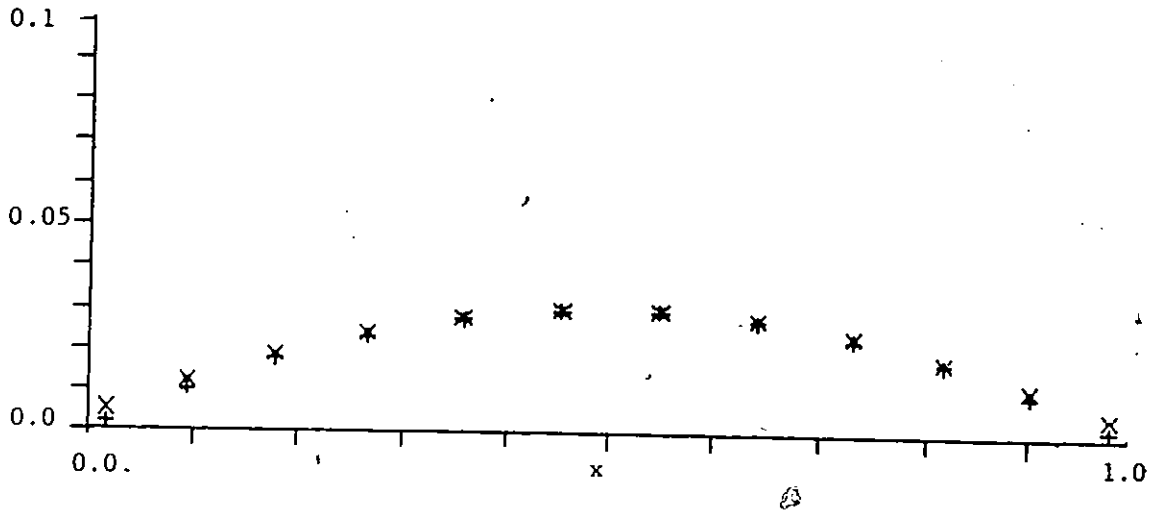

Fig. 17. A comparison between the body geometry calculated by the present method and exact body for a 6% circular arc airfoil at M_∞=0.817 in stretched coordinates.

\+ - exact

x - computed

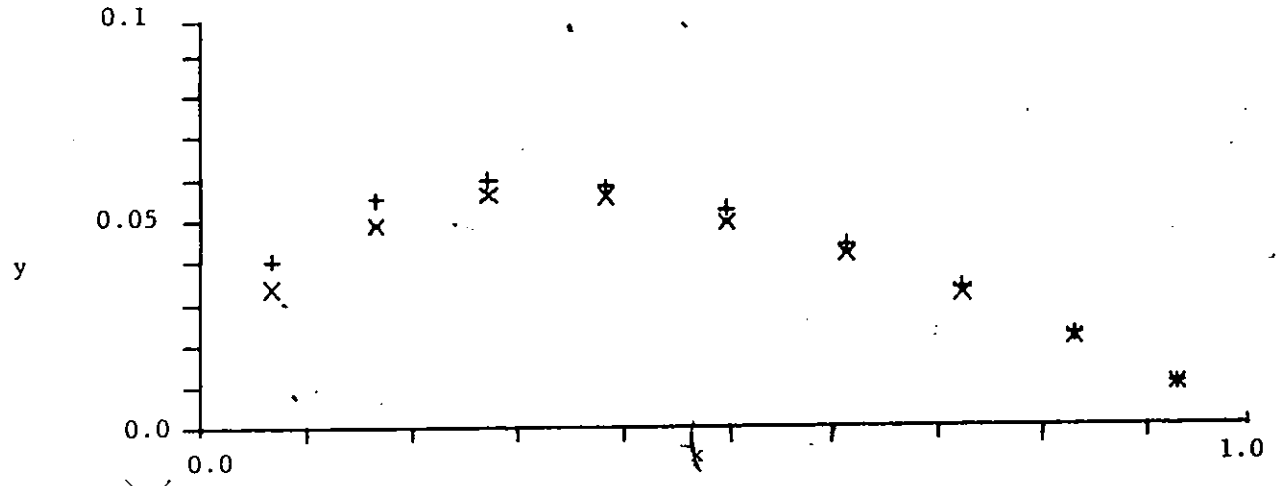

Fig. 18. A comparison between the body geometry calculated by the present method and exact body for NACA 0012 airfoil at M_∞=0.8 in un-stretched coordinates.

+ - exact

x - computed

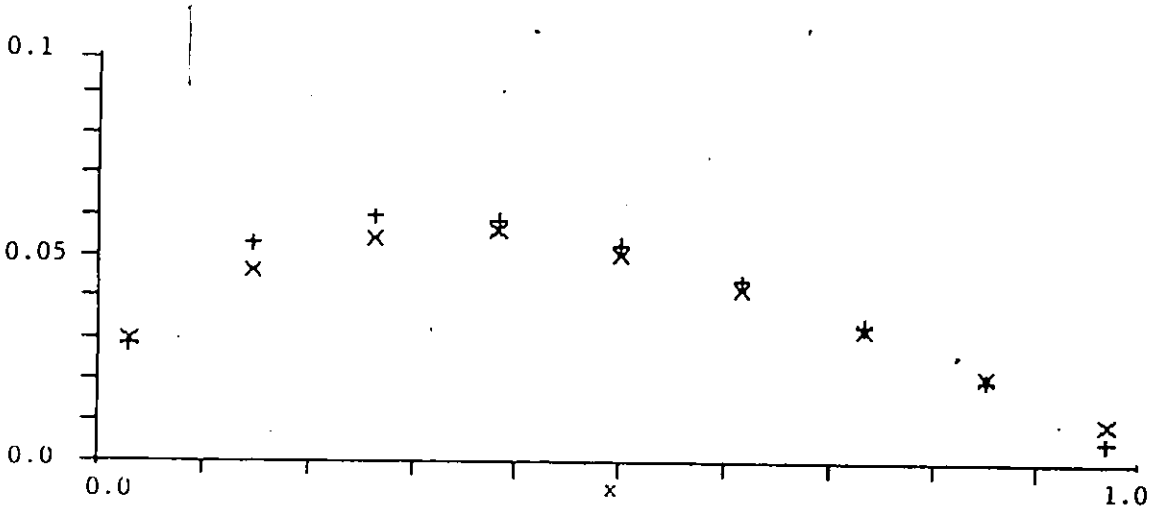

Fig. 19. A comparison between the body geometry calculated by the present method and exact body for NACA 0012 airfoil at M_∞=0.8 in stretched coordinates.

+ - exact

x - computed

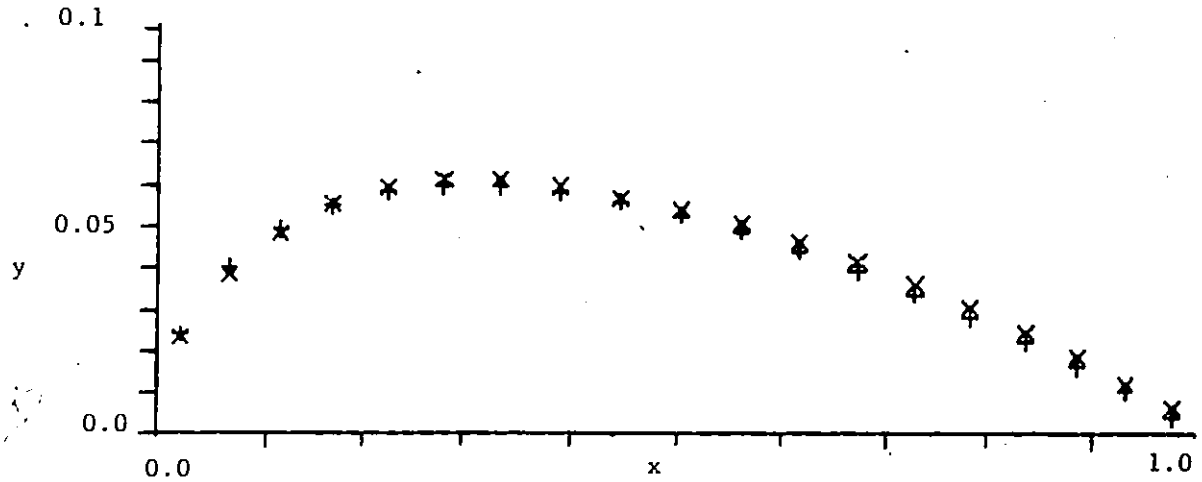

Fig. 20. A comparison between the body geometry calculated by the present method and exact body for NACA 0012 airfoil at M_∞=0.8 in stretched coordinates.

\+ - exact

x - computed

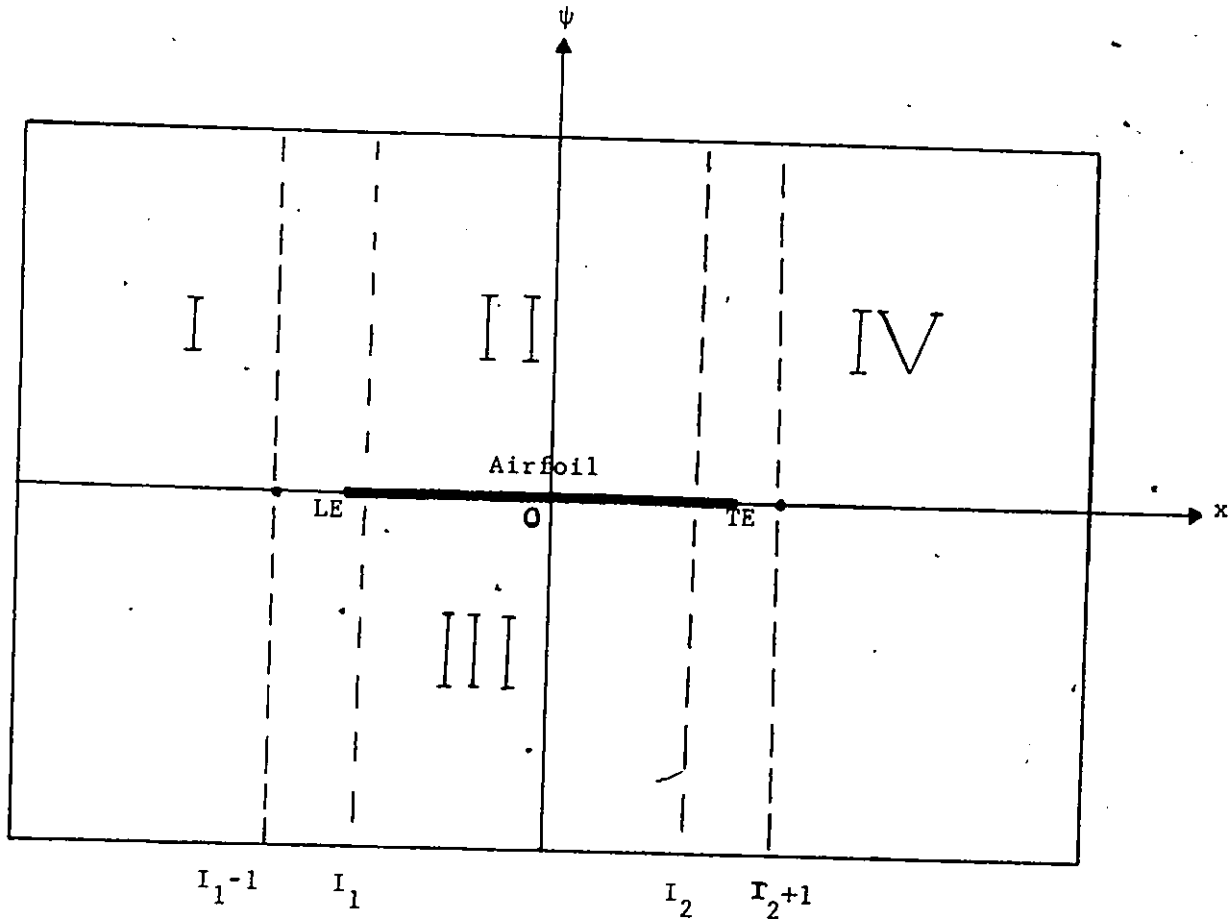

Fig. 21. The computacional domain in (x,ψ) system

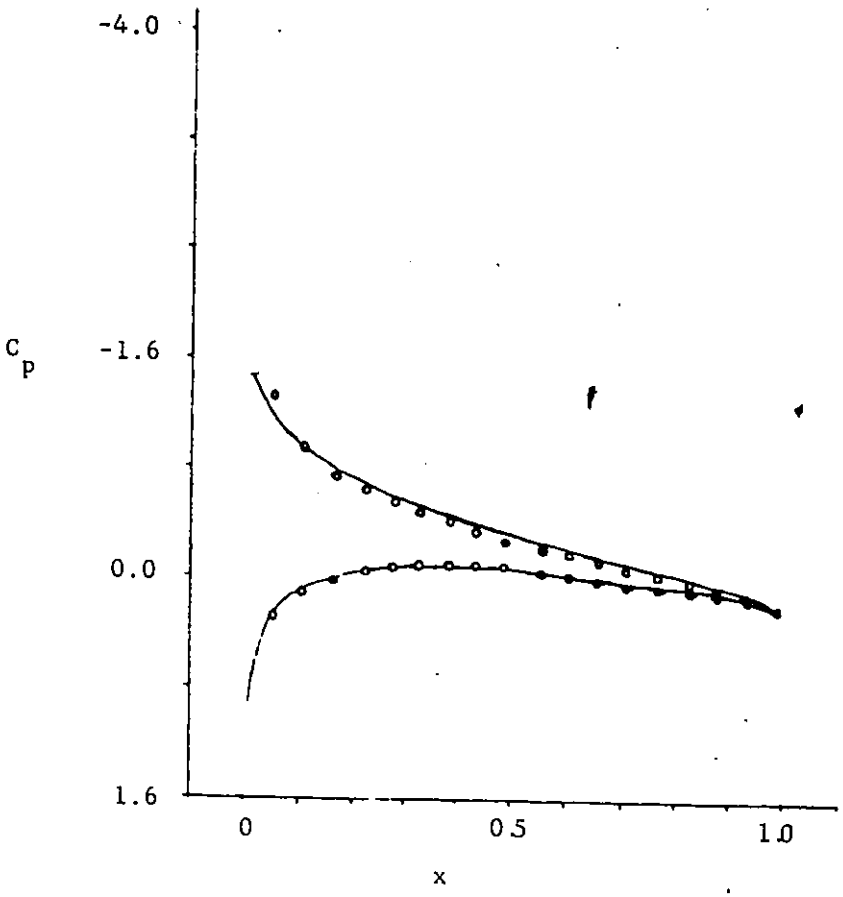

Fig. 22. Surface pressure distribution on NACA 0012 at $\alpha = 4°$.

—— Carey, Kim [42]

• Present method

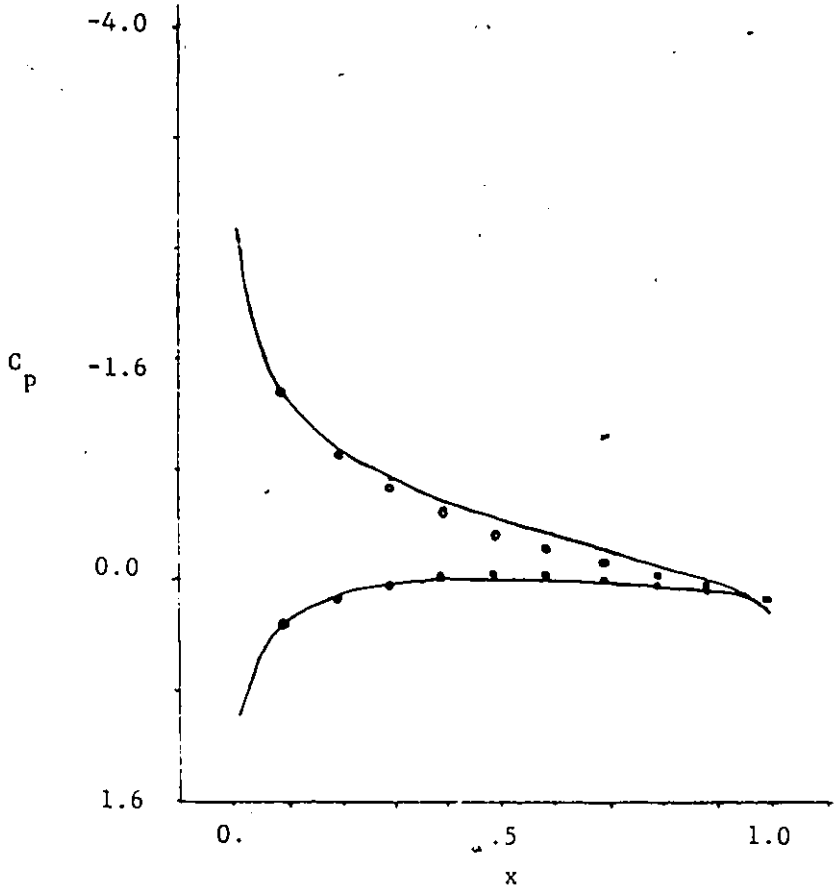

Fig. 23. Surface pressure distribution on NACA 0012 $\alpha = 6°$

—— Carey, Kim [42]

• Present method

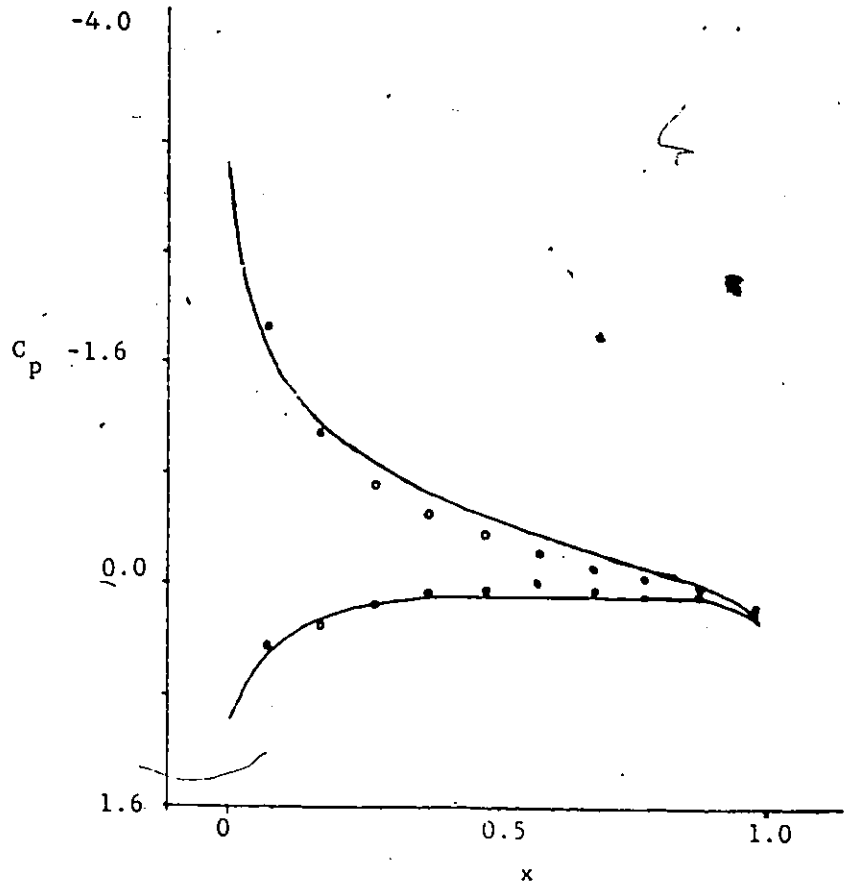

Fig. 24 Surface pressure distribution on NACA 0012 $\alpha=8°$

—— Carey, Kim [42]

• Present method

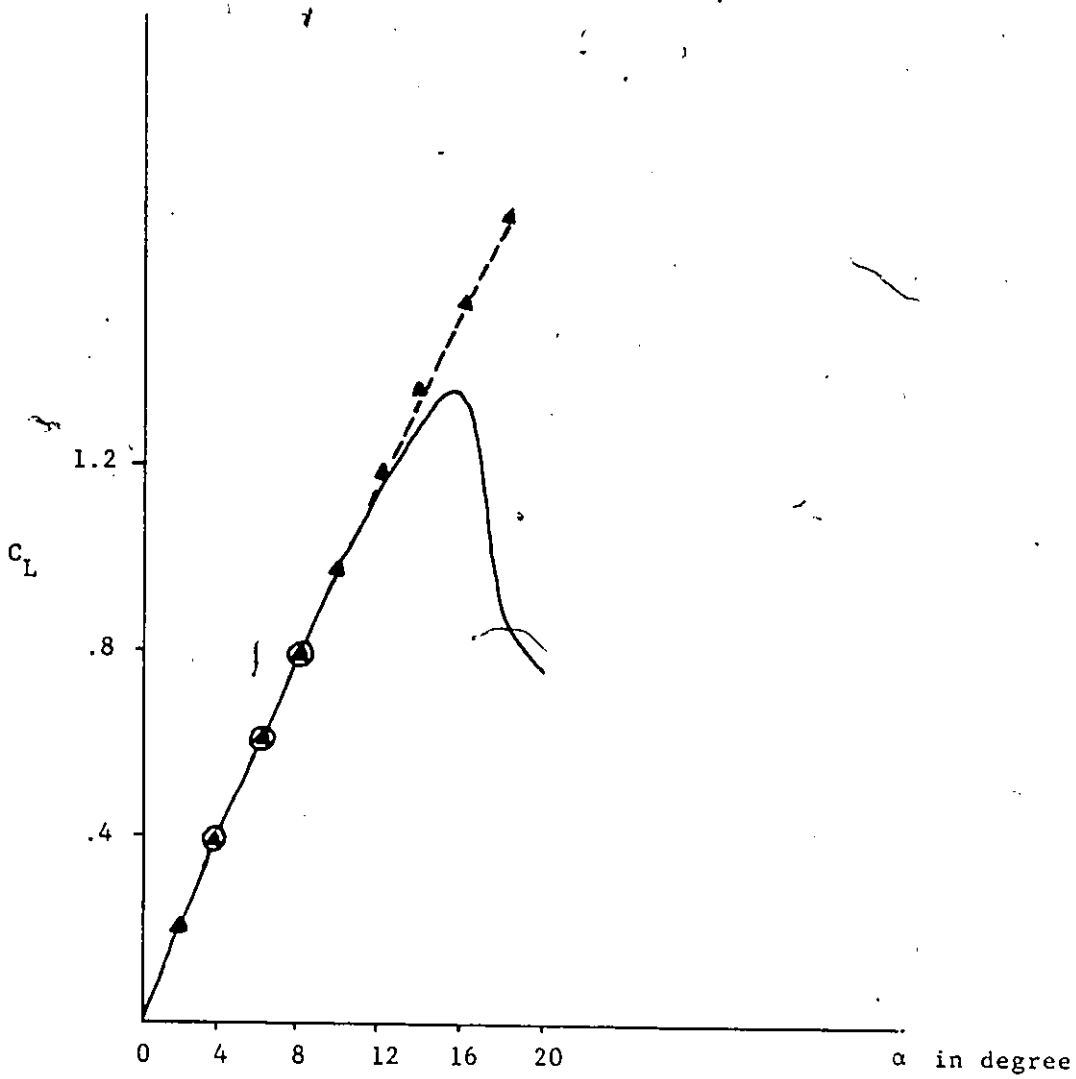

Fig. 25. Comparison of computed lift coefficient C_L with experimental results (incompressible)

—— Abbott and Doenhoff [43]

- - - Carey and Kim [42]

o Present method

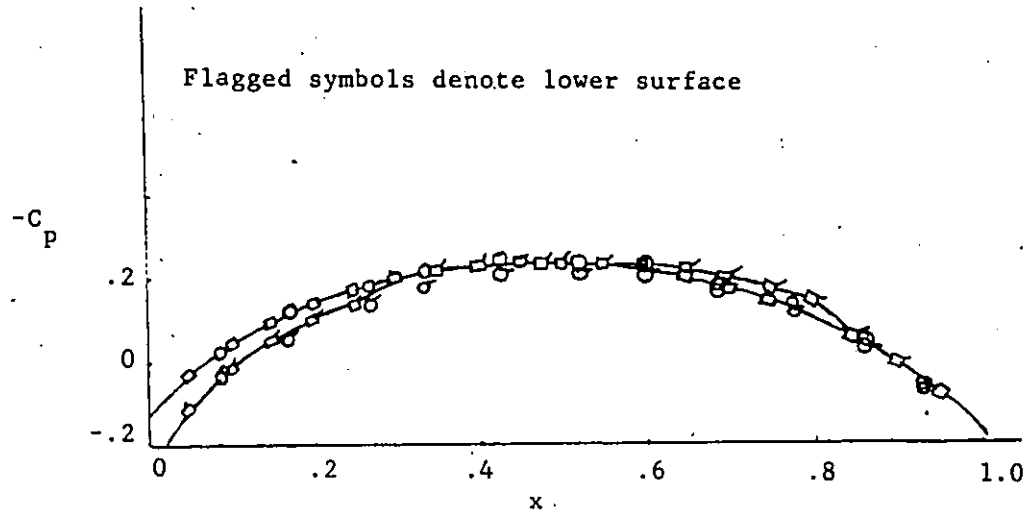

Fig. 26. Representative pressure distributions for 6% circular arc airfoil, M_∞=0.706, α=.5°

-□- Earl [35] experimental

o Present method

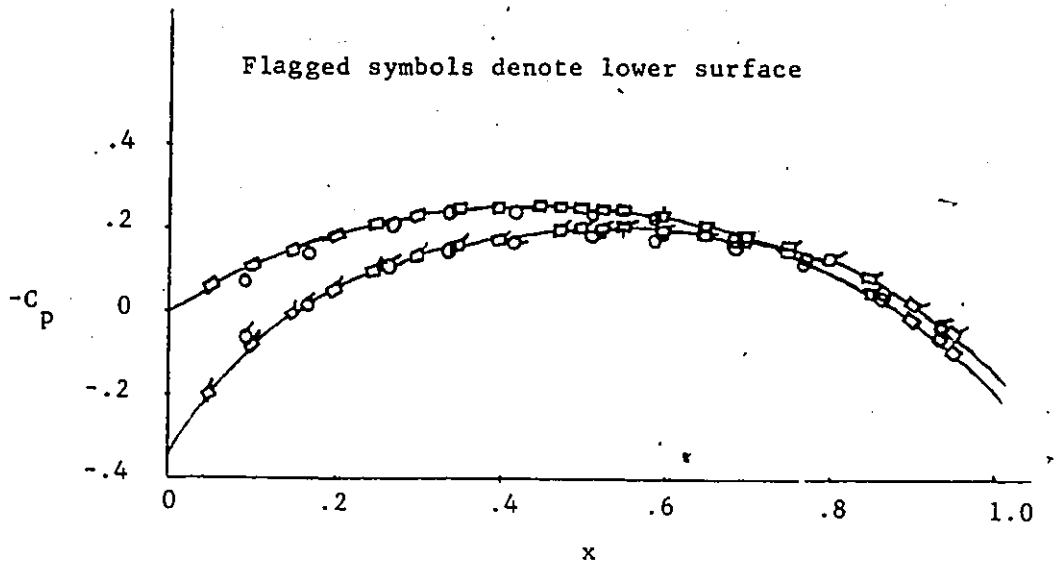

Fig. 27. Representative pressure distributions for 6% circular arc airfoil, M_∞=0.706, α = 1°

-□- Earl [35] experimental

o Present method

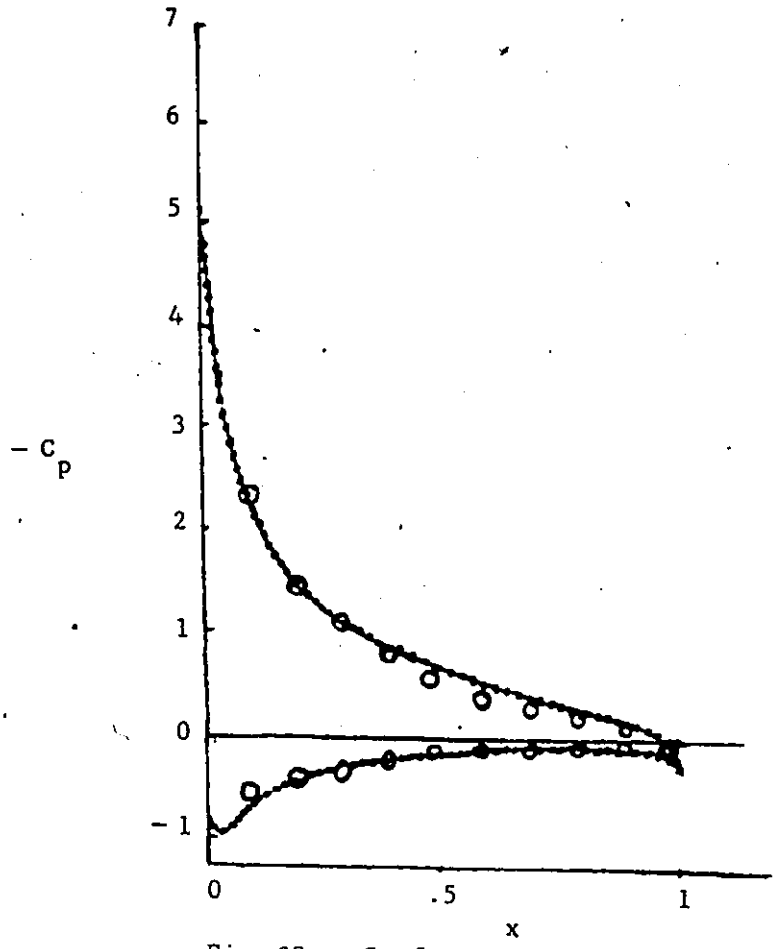

Fig. 28. Surface pressure distribution on NACA 0012 at $M_\infty = 0.3$, $\alpha = 10°$

• Hafez, et al. [41]

—— Classical Potential [c.f.(41)]

o Present method

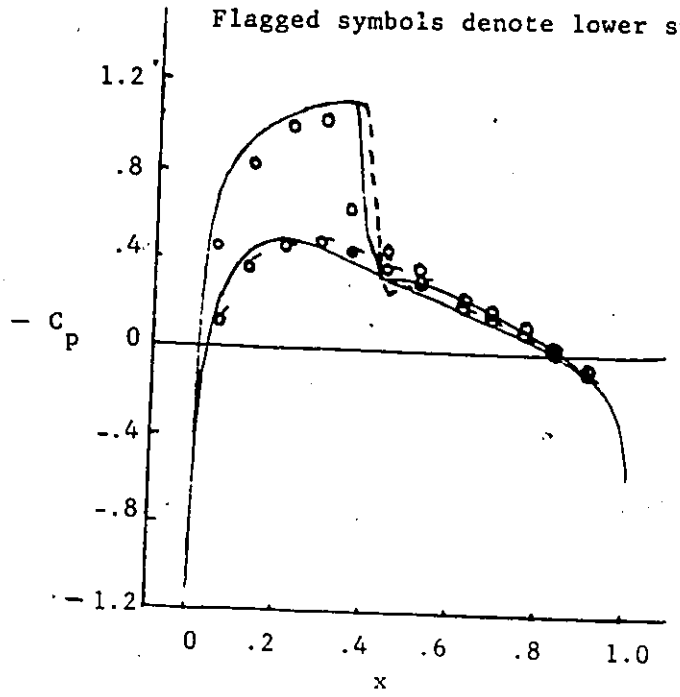

Fig. 29. Pressure coefficient comparison NACA0012 airfoil, M_∞=0.75; α =1°

- - - Holst [45]

——— Holst [45]

o Present method

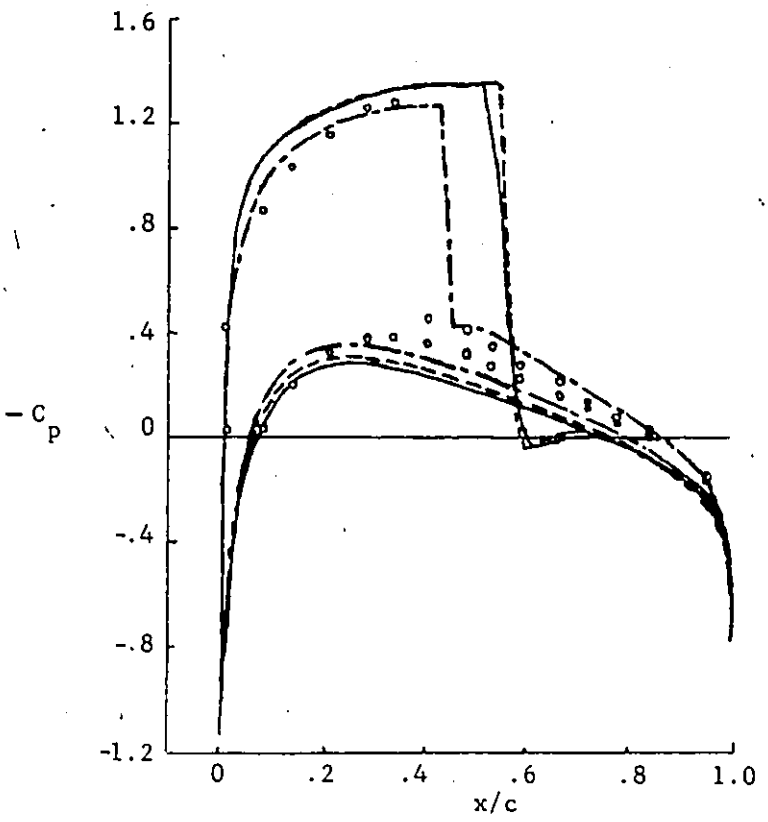

Fig. 30. Pressure coefficient NACA 0012, M_∞=0.75, α=2°

——— Holst[45]
- - - Conservative [c.f. (45)]
—.— Bauer et al. [46] (non-conservative)
0 Present method

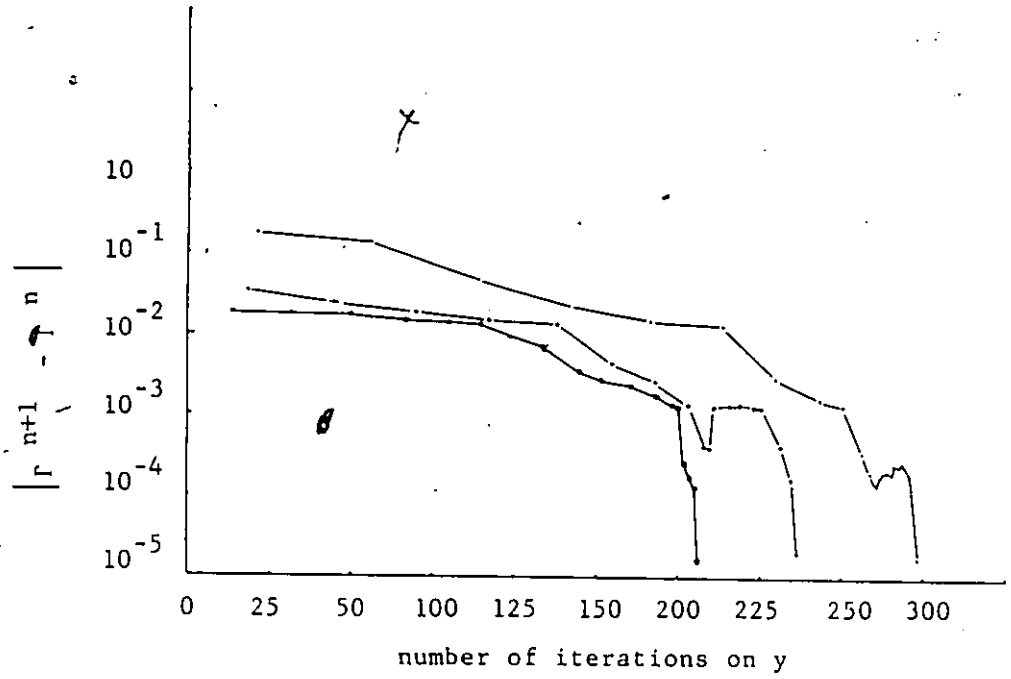

Fig. 31. Convergence history for Γ; NACA 0012

-o- $\alpha=1°$, $M_\infty=0.75$

-+- $\alpha=2°$, $M_\infty=0.75$

-·- $\alpha=10°$, $M_\infty=0.3$

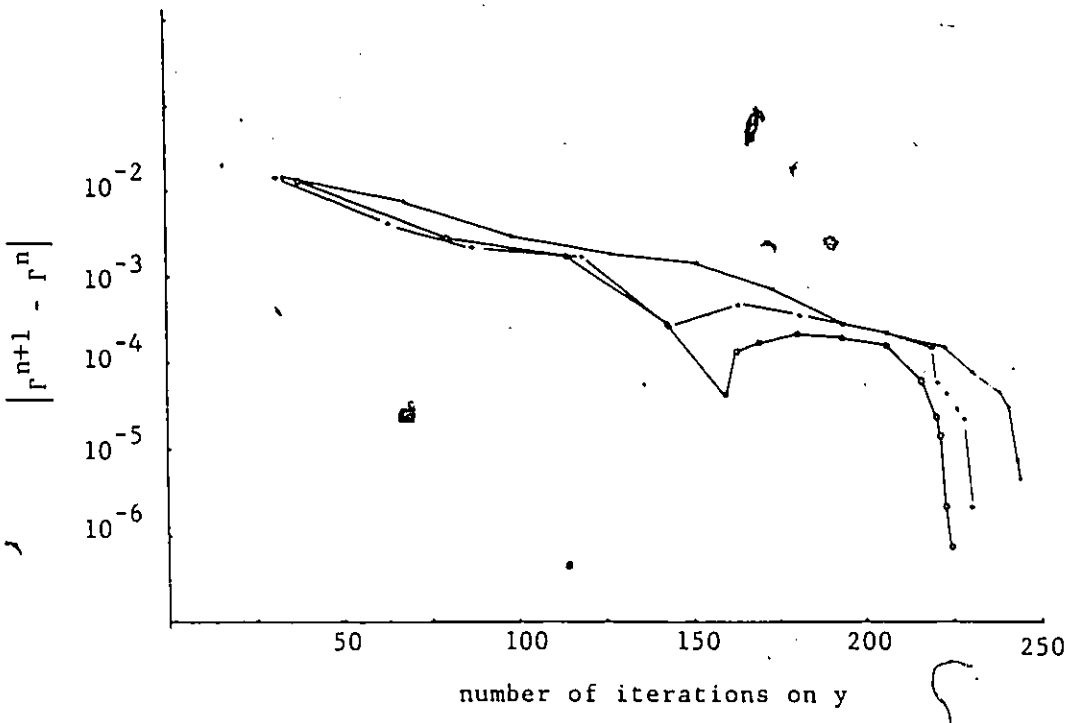

Fig. 32. Convergence history for D; NACA 0012, incompressible.

o $\alpha=4°$

\+ $\alpha=6°$

· $\alpha=8°$

TABLES

Table 1

Computational Information - NACA 0012 Airfoil
Direct Problem

Nature of Grid	Mach No.	Computational Domain	Grid Size	# of Iterations for y or Y	#of Iterations for ρ and $\tilde{\rho}$	C.P.U. Time (Seconds)
Un-stretched	0.63	$\{-7,7\} U \{0,4\}$	70 x 36	38	16	92.14
	0.7	$\{-7,7\} U \{0,4\}$	70 x 30	53	25	109.09
	0.8	$\{-2,2\} U \{0,3\}$	35 x 10	70	44	22.24
Stretched	0.63	$\{-1.5342780, 1.5342780\} U \{0,1.5042270\}$	25 x 18	35	14	13.74
	0.7	$\{-1.5342780, 1.5342780\} U \{0,1.5042270\}$	35 x 18	48	23	22.81
	0.8	$\{-1.5342780, 1.5342780\} U \{0,1.5042270\}$	25 x 10	94	56	21.02

U: Union

Table 2

Computational Information - 6% Circular Arc Airfoil
Direct Problem

Nature of Grid	Mach No.	Computational Domain	Grid Size	# of Iterations for y or Y	# of Iterations for ρ and $\tilde{\rho}$	C.P.U. Time (Seconds)
Un-stretched	0.817	$\{-2, 2\} \cup \{0,4\}$	100 x 11	53	41	27.60
Stretched	0.817	$\{-1.5342780, 1.5342780\} \cup \{0, 1.5042270\}$	59 x 6	454	25	168.86 *

* Tolerance used for y is 1×10^{-5}.

Table 3

Computational Information - Compressible, Fine Grid Solution

Airfoil	Mach. No.	Grid Size	# of iterations for y	# of iterations for ρ	CPU time (sec)
NACA 0012	0.53	170 x 10	261	104	160.3
	0.7	170 x 13	331	173	191.4
	0.8	90 x 30	292	167	286.8
6% circular arc	0.817	170 x 12	273	164	156.12

Table 4

Computational Information - NACA 0012 Airfoil
Inverse Problem

Nature of Grid	Mach No.	Grid Size	# of Iteration for y or Y	# of Iteration for ρ or $\tilde{\rho}$	C.P.U. Time (seconds)
Un-stretched	0.63	50 x 36	38	12	59.22
	0.7	70 x 30	47	12	90.33
	0.8	35 x 10	66	27	19.04
Stretched	0.63	25 x 18	41	12	16.01
	0.7	35 x 15	53	15	22.79
	0.8	25 x 10	98	34	20.60
	0.8	49 x 16	130	52	94.25

Table 5

Computational Information - 6% Circular Arc Airfoil
Inverse Problem

Nature of Grid	Mach No.	Grid Size	# of Iterations for y or Y	# of Iterations for ρ or $\tilde{\rho}$	C.P.U. Time (seconds)
Un-stretched	0.817	40 x 20	42	16	30.0
Stretched	0.817	30 x 6	44	16	06.79

Table 6

Computational Information - Compressible, Lifting Problem

Airfoil	α	β_o	M_∞	Grid Size	Computational Domain	# of Iteration for y	# of Iteration for Density ρ, $\tilde{\rho}$	# of Iteration for Circulation
6% Circular Arc	.5°	.25	.706	31x21	(-.7,1.9) U(-1.65, 1.65)	122	31	30
		.25	.706	31x21	(-.7,1.9) U(-1.63, 1.63)	143	20	19
NACA 0012	10°	.29	.3	32x19	(-1.1,2) U(-1.6, 1.6)	223	23	22
	1°	.25	.75	32x29	(-.83,1.65) U(-1.5,1.5)	156	17	16
	2°	.27	.75	48x21	(-1.6,1.6) U(-1.,2.)	187	18	17

Table 7

Computational Information Incompressible, NACA 0012 Airfoil Lifting Problem

α	β_o	Grid Size	Computational Domain	# of Iterations for y	# of iterations for circulation
4°	.27	91 x 35	(-2.,3) U(-1.15, 1.15	225	14
6°	.27	51 x 19	(-2.,3) U(-1.15,1.15)	231	14
8°	.27	51 x 21	(-2.,3) U(-1.16,1.16)	244	13

DIAGRAMS

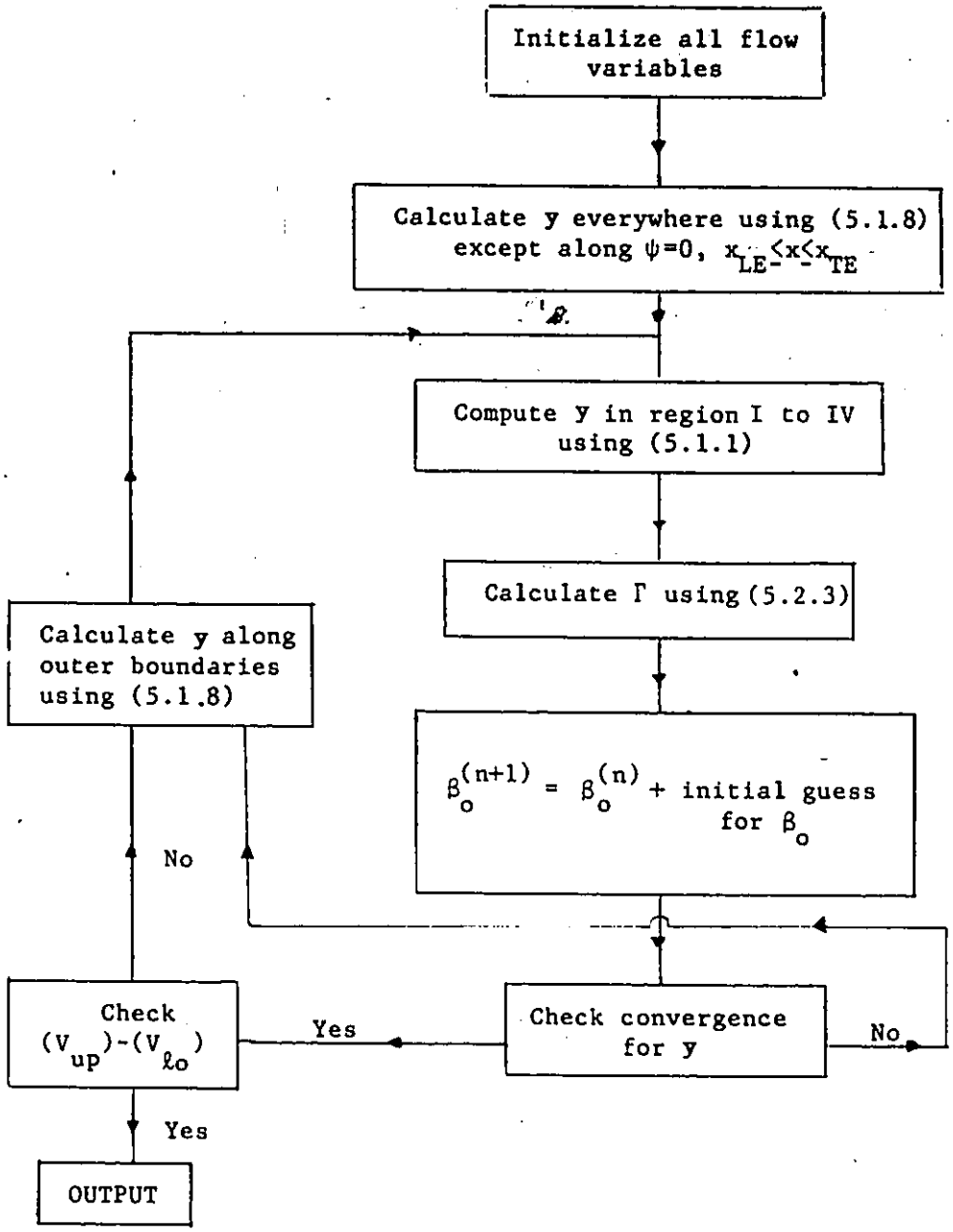

Diagram 1. Determination of β_o

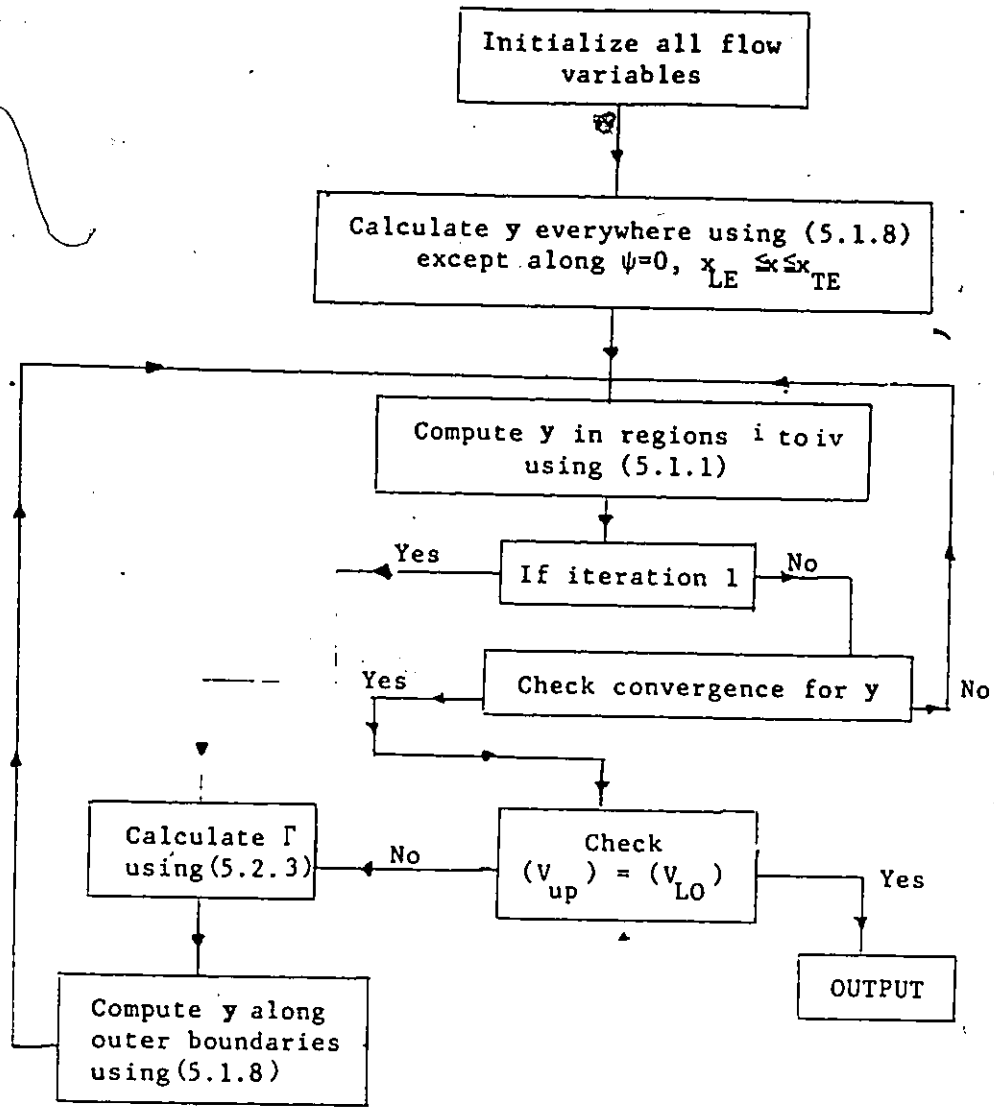

Diagram 2. Determination of Flow Field for Incompressible Case

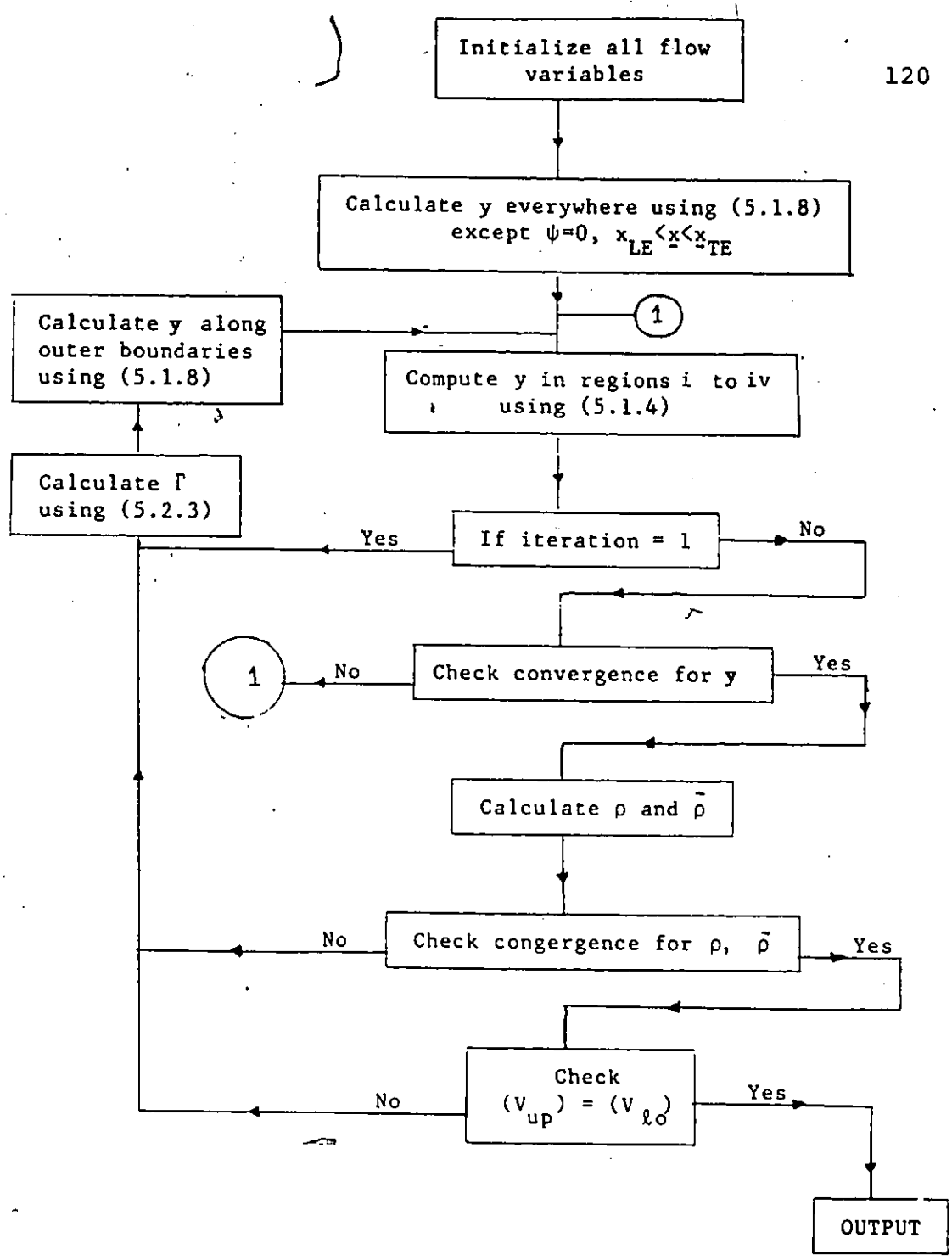

Diagram 3. Determination of Flow Field for Compressible Case

REFERENCES

[1] SPEE, B. M., Investigations on the Transonic Flow around Aerofoils, NLR, TR 69122U, 1969.

[2] PEARCEY, H. H., Contribution to Round Table Discussion at AGARD Specialists Meeting on Transonic Aerodynamics, AGARD Suppl. CP35, 1968.

[3] NIEUWLAND, G. Y., SPEE, B. M., Transonic Shock-free Flow, Fact or Fiction? Trans. Aerodynam., AGARD Conf. Proc. No. 35, 1968.

[4] BOERSTOEL, J. W., UIJLENHOET, R., Lifting Aerofoils with Supercritical Shock-free Flow, ICAS Paper No. 70-15, 1970.

[5] PEYRET, R., THOMAS, D. T., Computational Methods for Fluid Flow, Springer Verlag Publ. Inc., N.Y., 1985.

[6] OSWATITSCH. K., KUERTI, G., Gas Dynamics, Academic Press, N. Y., 1956.

[7] CHENG, H. K., The Transonic-Flow Theories of High and Low-Aspect Ratio Wings, Symposium on Numerical and Physical Aspects of Aerodynamics Flows, California State University, January, 1981.

[8] McCORMICK, B. W., Aerodynamics, Aeronautics and Flight Mechanics, Academic Press, N. Y., 1964.

[9] VAN DYKE, M., Perturbation Methods in Fluid Mechanics, Academic Press, N. Y., 1964.

[10] HAFEZ, M., Perturbation of Transonic Flow with Shocks, Symposium on Numerical and Physical Aspects of Aerodynamics Flows, California State University, January, 1981.

[11] MURMAN, E.M., COLE, J.D., Calculation of Plane Steady Transonic Flows, AIAA Journal, Vol. 9, No. 1, pp. 114-121, 1971.

[12] BALLHAUS, W.F., BAILEY, F.R. AIAA Paper 72-677, 1972.

[13] STEGER, J. L., LOMAX, H., Transonic Flow about Two Dimensional Airfoils by Relaxation Procedures, AIAA Journal, Vol. 10, No. 1, pp. 49-54, 1972.

[14] GARABEDIAN, P. R., KORN, D., Analysis of Transonic Airfoils, Comm. Pure Appl. Math., Vol. 24, pp. 841-851, 1971.

[15] CAUGHEY, D.A., JAMESON, A., Numerical Calculation of Transonic Potential Flow about Wing-Body Combinations, AIAA Journal, Vol. 17, No. 2, pp. 175-214, 1979.

[16] JAMESON, A., CAUGHEY, D.A., A Finite Volume Method for Transonic Potential Flow Calculations, AIAA Conference, Albuquerque, New Mexico, June 1977.

[17] HABASHI, W.G., HAFEZ, M.H., Finite Element Solutions of Transonic Flow Problems, AIAA Journal, Vol. 20, No. 10, pp. 1368-1376, 1982.

[18] JAMESON, A., Transonic Flow Calculations, VKI Lecture Series 87, Computational Fluid Dynamics, March, 1976.

[19] HAFEZ, M., LOVELL, D., Numerical Solution of Transonic Stream Function Equation, AIAA Journal, Vol. 21, No. 3, pp. 327-334, 1983.

[20] WONG, Y.S., HAFEZ, M., Conjugate Gradient Method Applied to Transonic Finite Difference and Finite Element Calculations, AIAA Journal, Vol. 20, No. 11, pp. 1526-1533, 1982.

[21] THOMPSON, J.F., WARSI, Z.U., MASTIN, C.W., Numerical Grid Generation; Foundations and Application, North Holland, N.Y., 1985.

[22] MARTIN, M.H., The Flow of a Viscous Fluid I, Arch. of Rat. Mech. and Analysis, 41, pp. 266-286, 1971.

[23] GROSSMAN, G.W., BARRON, R.M., A New Approach to the solution of Navier-Stokes Equations, Int. J. Num. Methods in Fluids, Vol. 17, No. 12, pp. 1315-1324, 1987.

[24] BARRON, R.M., Computation of Incmpressible Potential Flow using von Mises Coordinates, in Mathematics and Computers in Simulation.

[25] MURMAN, E.M., Analysis of Embedded Shock Waves Calculated by Relaxation Method, AIAA Journal, Vol. 12, No. 5, pp. 626-633, 1973.

[26] JAMESON, A., Iterative Solution of Transonic Flows

over Airfoils and Wings, Comm. Pure Appl. Math. Vol. 2, pp. 283-309, 1974.

[27] JAMESON, A., Transonic Potential Flow Calculation using Conservative Form, Proceedings of the AIAA Second Computational Fluid Dynamics Conference, Hartford, Conn., June, pp. 148-161, 1975.

[28] HARTEN, A., The Artificial Compression Method for Computation of Shocks and Contact Discontinuities, ICASE Report No. 77-2, Feb., 1977.

[29] JAMESON, A., Numerical Computation of Transonic Flows with Shock Waves, Symposium Transsonicum II, Springer Verlag, N.Y., 1976.

[30] HAFEZ, M., MURMAN, E.M., SOUTH, J., Artificial Compressibility Methods for Numerical Solution of the Transonic Full Potential Equation, AIAA Paper 78-1148, 1978.

[31] JONES, D.J., DICKINSON, R.G., A Description of the NAE Two-Dimensional Transonic Small Disturbance Computer Method, NAE Laboratory Technical Report LTR-HA-39, Jan., 1980.

[32] ESSERS, J.A., Evolution Approaches to the Numerical Treatment of Inviscid Internal Flows, Computational Fluid Dynamics. Edited by Wolfgang Kollman, McGraw-Hill International Book Company, N.Y., 1980.

[33] SINCLAIR, P.M., An Exact Integral (field Panel) Method for the Calculation of Two Dimensional Transonic Potential Flow around Complex Configurations, Aeronautical Journal, Vol. 90, No. 896, pp. 227-236, 1986.

[34] WIGTON, L.B., Application of MACSYMA and Sparse Matrix Technology to Multielement Airfoil Calculations, AIAA Paper 87-1142, 1987.

[35] EARL, D.K., Experimental Investigation at Transonic Speeds of Pressure Distributions over Wedge and Circular Arc Airfoil Sections and Evaluation of Perforated Wall Interference, NASA, TN D-15. 1959.

[36] HABASHI, W.G., KOTIUGA, P.L., McLEAN, L.A., Finite Element Simulation of Transonic Flows by Modified Potential and Stream Function Methods, Engineering Analysis, Vol. 2, No. 3, 1986.

[37] HESS, J.L., SMITH, A.M.O., Calculation of Potential Flow about Arbitrary Bodies, Progress in Aeronautical Sciences, Vol. 8, Pergamon Press, N.Y., 1967.

[38] MARSHALL, F.J., Design Problem in Hydrodynamics, Journal of Hydronautics, Vol. 4, October, pp. 136-139, 1970.

[39] von KARMAN, T., Calculation of the Flowfield around Airships, NASA TM574, July 1930.

[40] ATKINS, H.L. and HASSAN, H.A., A new Stream Function Formulation for the steady Euler Equations, AIAA J.23 No. 5, pp. 701-706, 1985.

[41] HAFEZ, M., HABASHI, W.G., KOTIUGA, P.L., Short Communication: Conservative Calculations of Non-isentropic Transonic Flows, International Journal for Numerical Methods in Fluids, Vol. 5, pp. 1047-1057, 1985.

[42] CAREY, G.F., KIM, S.W., Lifting Aerofoil Calculation using the Boundary Element Method, International Journal for Numerical Methods in Fluids, Vol. 3, pp. 481-482, 1983.

[43] ABBOTT, I.H., von DOENHOFF, A.E., Theory of Wing Sections, Dover Publications, N.Y., 1959.

[44] HOLST, T.L., Fast, Conservative Algorithm for Solving the Transonic Full-potential Equation, AIAA Journal, Vol. 18, No. 12, pp. 1431-1439, 1980.

[45] HOLST, T.L., Implicit Algorithm for the Conservative Transonic Full-potential Equation using an Arbitrary Mesh, AIAA Paper, Art. No. 78-1113R, 1978.

[46] BAUER, F., GARABEDIAN, P., KORN, D., JAMESON, A., Supercritical Wing Section, Lecture Notes in Economics and Mathematical System, 108, Springer Verlag, 1975.

[47] CHANDNA, O.P., BARRON, R.M. and GARG, M.R., Plane Compressible MHD Flows, Q. of Appl. Math., Vol. 26, No. 3, pp. 411-422, 1979.

[48] NAEEM, R.K., On Exact Solutions for Navier-Stokes Equations, M.Sc. Major Paper, Dept. of Mathematics and Statistics, U. of Windsor, Windsor, Ont., 1984.

VITA AUCTORIS

The author was born in Karachi, Pakistan in 1955. He received his M.Sc. in Applied Mathematics from the University of Karachi in 1979. He joined the Department of Mathematics, University of Karachi, as a cooperative teacher in 1980 and received permanent lecturership in 1983. He also taught as a part-time teacher at the Department of Mathematics, NED University of Engineering, Karachi, for one semester in 1982. In September 1983 he resigned from his position and came to Windsor. In 1984 he received a M.Sc. in Applied Mathematics from the University of Windsor, Windsor, Ontario, Canada.